The Astrophysical Journal, 841:98 (16pp), 2017 June 1 https://doi.org/10.3847/1538-4357/aa6f5b

Radio Pulse Search and X-Ray Monitoring of SAX J1808.4−3658: What Causes Its Orbital Evolution?

Alessandro Patruno[1,2], Amruta Jaodand[2,3], Lucien Kuiper[4], Peter Bult[3,5], Jason W. T. Hessels[2,3], Christian Knigge[6], Andrew R. King[1,3,7], Rudy Wijnands[3], and Michiel van der Klis[3]
[1] Leiden Observatory, Leiden University, Neils Bohrweg 2, 2333 CA, Leiden, The Netherlands
[2] ASTRON, the Netherlands Institute for Radio Astronomy, Postbus 2, 7900 AA, Dwingeloo, The Netherlands
[3] Anton Pannekoek Institute for Astronomy, University of Amsterdam, Science Park 904, 1098 XH, Amsterdam, The Netherlands
[4] SRON-National Institute for Space Research, Sorbonnelaan 2, NL-3584 CA, Utrecht, The Netherlands
[5] Astrophysics Science Division, NASA Goddard Space Flight Center, Greenbelt, MD 20771, USA
[6] University of Southampton, School of Physics and Astronomy, Southampton SO17 1BJ, UK
[7] Theoretical Astrophysics Group, Department of Physics and Astronomy, University of Leicester, Leicester LE1 7RH, UK
Received 2016 November 12; revised 2017 April 21; accepted 2017 April 23; published 2017 May 30

Abstract

The accreting millisecond X-ray pulsar SAX J1808.4−3658 shows a peculiar orbital evolution that proceeds at a very fast pace. It is important to identify the underlying mechanism responsible for this behavior because it can help to understand how this system evolves and which physical processes (such as mass loss or spin–orbit coupling) are occurring in the binary. It has also been suggested that, when in quiescence, SAX J1808.4−3658 turns on as a radio pulsar, a circumstance that might provide a link between accreting millisecond pulsars and black-widow (BW) radio pulsars. In this work, we report the results of a deep radio pulsation search at 2 GHz using the Green Bank Telescope in 2014 August and an X-ray study of the 2015 outburst with *Chandra*, *Swift* XRT, and *INTEGRAL*. In quiescence, we detect no radio pulsations and place the strongest limit to date on the pulsed radio flux density of any accreting millisecond pulsar. We also find that the orbit of SAX J1808.4−3658 continues evolving at a fast pace. We compare the orbital evolution of SAX J1808.4−3658 to that of several other accreting and nonaccreting binaries, including BWs, redbacks, cataclysmic variables, black holes, and neutron stars in low-mass X-ray binaries. We discuss two possible scenarios: either the neutron star has a large moment of inertia and is ablating the donor, generating mass loss with an efficiency of 40%, or the donor star has a strong magnetic field of at least 1 kG and is undergoing quasi-cyclic variations due to spin–orbit coupling.

Key words: binaries: general – stars: individual (SAX J1808.4-3658) – stars: neutron – stars: rotation – X-rays: binaries – X-rays: stars

1. Introduction

The accreting millisecond X-ray pulsar (AMXP) SAX J1808.4−3658 is an accreting neutron star located at a distance of 3.5 kpc (Galloway & Cumming 2006) that is spinning at 401 Hz (Wijnands & van der Klis 1998) and orbiting its 0.05–0.08 $M_{\odot}$ companion in 2.01 hr (Chakrabarty & Morgan 1998; Deloye et al. 2008; Wang et al. 2013). This source was discovered by *BeppoSAX* in 1996 (in't Zand et al. 1998) and is the best-studied AMXP of all 18 known members (see Patruno & Watts 2017 for a review). It has shown eight outbursts so far, observed with a recurrence time of approximately 3–4 yr. The high time and/or spectral resolution of X-ray telescopes such as the *Rossi X-Ray Timing Explorer* (*RXTE*), *XMM-Newton*, *International Gamma-Ray Astrophysics Laboratory* (*INTEGRAL*), *Chandra*, *Swift*, and *Suzaku* has allowed a thorough study of the pulsations (see, e.g., Hartman et al. 2008; Burderi et al. 2009; Patruno et al. 2012), aperiodic timing variability (Wijnands et al. 2001, 2003; Patruno et al. 2009c; Bult & van der Klis 2015), and X-ray spectral properties (Gierliński et al. 2002; Poutanen & Gierliński 2003; Cackett et al. 2009; Papitto et al. 2009; Patruno et al. 2009b).

The coherent timing of the pulsations has revealed the lack of a strong spin-up during the outbursts (Hartman et al. 2008, 2009) and a constant spin-down in quiescence that is compatible with magnetic dipole energy loss (surface magnetic field $B \approx 10^8$ G; see di Salvo et al. 2008; Hartman et al. 2008, 2009; Patruno et al. 2012). There is also indirect observational evidence that SAX J1808.4−3658 turns on as a radio pulsar during quiescence, although no radio pulsations have been detected so far (Homer et al. 2001; Burderi et al. 2003; Campana et al. 2004; Iacolina et al. 2010). Indeed, the optical counterpart of SAX J1808.4−3658 is overluminous with respect to a nonirradiated brown-dwarf model (Bildsten & Chakrabarty 2001) during this phase. A source of irradiation is required to explain this behavior, but the feeble X-ray irradiation coming from the accretion disk/neutron star surface during quiescence (Homer et al. 2001; Heinke et al. 2009) cannot account for the donor luminosity. It has been speculated that a pulsar wind impinging on the donor surface (Burderi et al. 2003; Campana et al. 2004) might be responsible for the observed excess luminosity.[8] Optical modulation at the orbital period is now well established in black-widow (BW) and redback radio pulsar systems (Breton et al. 2013), and something similar has been found for SAX J1808.4−3658 during quiescence (Deloye et al. 2008; Wang et al. 2013).

In recent works, Xing et al. (2015) and de Oña Wilhelmi et al. (2016) identified a possible gamma-ray counterpart of SAX J1808.4−3658, and spectral modeling of the Fermi Large Area Telescope (*FERMI*/LAT) data implies that (if the

[8] Although the requirement of a pulsar wind is often mentioned as indirect evidence for a radio pulsar turning on, it is also possible that a pulsar wind is active without the radio pulsar mechanism operating in the system (or at least without radio pulsations being observable, as they may be obscured by intra-binary material; see, e.g., Jaodand et al. 2016).

counterpart is confirmed) about 30% of the spin-down energy is transformed into gamma rays, providing further evidence in favor of this scenario, although no gamma-ray pulsations have been found so far.

The orbital evolution of SAX J1808.4−3658 shows an increase of the orbital period on a relatively short timescale of ∼70 Myr (di Salvo et al. 2008; Hartman et al. 2008) and an acceleration of the rate of expansion of the orbit up to 2011 (Patruno et al. 2012). The driving mechanism for the evolution of a binary with an ∼2 hr orbital period like SAX J1808.4−3658 is expected to be angular momentum loss due to gravitational-wave emission. The expected orbital evolution timescale in this case is ∼4 Gyr (Hartman et al. 2008), which is almost two orders of magnitude longer than the observed one.

Anomalously fast orbital evolution is not unique to SAX J1808.4−3658. Several other low-mass X-ray binaries (LMXBs), comprising both neutron star and black hole accretors, are also observed to show a faster evolution than expected (see Section 6 for an in-depth discussion). There is a similar behavior in many (nonaccreting) binary radio millisecond pulsars with orbital parameters similar to those of SAX J1808.4−3658, known as BWs, where the rotational power emitted in the form of wind and radiation by the pulsar is impinging and ablating the semi-degenerate[9] donor companion (Nice et al. 2000; Doroshenko et al. 2001; Lazaridis et al. 2011; Shaifullah et al. 2016). These systems have a companion star with a typical mass of $\lesssim 0.1\,M_{\odot}$, and several (but not all) of them have orbital periods of about 1–3 hr. Most BWs have very short binary evolution timescales too, orders of magnitude shorter than the expected theoretical values for their secular evolution. These short-timescale variations are believed to reflect some short-term effects rather than the secular evolution of the binary.

For SAX J1808.4−3658, di Salvo et al. (2008) proposed a scenario in which the pulsar wind, powered by the rotational spin-down of the neutron star in quiescence, causes the ejection of the gas flowing through the inner Lagrangian point L_1 (radio-ejection scenario; see also Burderi et al. 2001, 2009). Hartman et al. (2008, 2009) and Patruno et al. (2012) proposed an alternative mechanism, in which the binary evolution is not necessarily driven by the matter expulsion but rather is a quasi-stochastic process due to the development of a significant mass quadrupole in the donor star that results in a coupling between the donor spin and the orbital period of the binary. Patruno et al. (2012) in particular showed that the Applegate mechanism (Applegate 1992; Applegate & Shaham 1994), which assumes that a mass quadrupole develops in the donor star due to quasi-periodic magnetic cycles, seems to be a promising candidate surviving the observational scrutiny. However, there is not yet any conclusive evidence about the exact operating mechanism behind the orbital evolution of SAX J1808.4−3658.

Motivated by these facts, we have conducted a deep radio pulse search of SAX J1808.4−3658 during quiescence and X-ray monitoring during the 2015 outburst. The deep radio pulse search was done with the Green Bank Telescope (GBT) in 2014 August (during quiescence) in order to answer the following question: does SAX J1808.4−3658 really turn on as a radio pulsar during quiescence? A detection could help solve two problems. The first is that it would allow continuous monitoring of the orbital evolution not only during outbursts but also during quiescence. The second is that it can allow the precise measurement of the spin-down power of the pulsar, which likely plays a fundamental role in the ablation of the companion. The X-ray monitoring campaign was made with the *Swift* X-Ray Telescope (XRT) and the *INTEGRAL* and *Chandra* telescopes during the 2015 outburst. We used the *Chandra* telescope to monitor the pulsations of the source and track the long-term orbital evolution of SAX J1808.4−3658. The question we seek to answer is whether the determination of a new orbital solution that includes the 2015 outburst can provide hints about the exact mechanism behind the rapid orbital evolution of the system.

2. X-Ray Observation and Data Reduction

To construct the outburst light curve, we analyzed all pointed *Swift* XRT observations taken between 2015 April 3 (MJD 57113) and 2015 August 26 (MJD 57260). During this period, 62 observations were taken (Program IDs 33737, 30034, and 33801) in either window-timing mode (1.76 ms resolution) or photon-counting mode (2.5 s). We extracted X-ray count rates averaged per spacecraft orbit using the online *Swift* XRT data products generator (Evans et al. 2007). To estimate the count rate–to–flux conversion ratio, we used this tool to create and fit energy spectra (Evans et al. 2009) using the 0.3–10 keV energy and the default event grades. One Type I (i.e., thermonuclear) X-ray burst was detected and excluded from our analysis (see Figure 1).

We also used data recorded with the *INTEGRAL* spacecraft (Winkler et al. 2003). Driven by sensitivity considerations, we only used data from the *INTEGRAL* Soft Gamma-Ray Imager (ISGRI; Lebrun et al. 2003)—the upper detector layer of Imager on Board the INTEGRAL Satellite (IBIS) (Ubertini et al. 2003)—sensitive to photons with energies in the range ∼20 keV–1 MeV (effectively ∼300 keV). Typical integration times are in the range 1800–3600 s. We used the imaging software tools (Goldwurm et al. 2003) of the Offline Scientific Analysis (OSA) package version 10.1, distributed by the *INTEGRAL* Science Data Centre (ISDC; see, e.g., Courvoisier et al. 2003). *INTEGRAL* had the Galactic center/bulge region in its field of view often during the 2015 April outburst of SAX J1808.4−3658, and the initial part of the outburst was properly sampled. The light curve for the 20–100 keV range during the early phase of the outburst is shown in Figure 2. Each data point represents the averaged count rate of a combination of typical 3–5 science windows.[10] The onset of the outburst, somewhat before MJD 57121, is clearly visible in the figure.

For the timing analysis, we used *Chandra* data taken with the High Resolution Camera (HRC) with the HRC-S detector operating in timing mode. The observation started on 2015 May 24 at 22:23:18 UT (MJD 57166.9) and ended on 2015 May 25 at 07:15:30 UT (MJD 57167.3), for a total exposure time of 29.6 ks. In this configuration, the data were collected with a time resolution of 16 μs and very limited energy resolution (Rutledge et al. 2004). The *Chandra* data were processed with the CIAO software (version 4.6) and barycentered with the *faxbary* tool by using the most precise optical position available (Hartman et al. 2008) and the JPL DE405 solar system ephemeris. The pulse profiles were generated by

[9] In this paper, we use the term "semi-degenerate" instead of "brown dwarf" because the mass transfer process significantly alters the internal structure of these stars, which are quite different from isolated brown dwarfs (Tauris 2011).

[10] A science window is a continuous time interval during which the data is acquired by the *INTEGRAL* instruments.

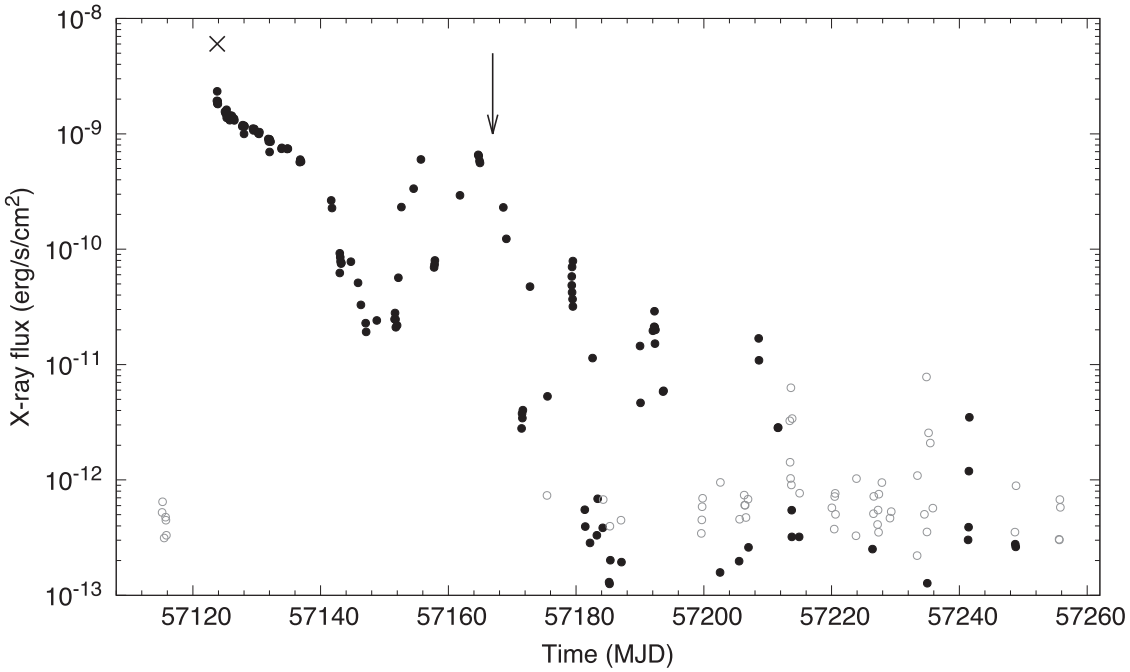

Figure 1. X-ray light curve (0.3–10 keV) of SAX J1808.4−3658 obtained with the *Swift* XRT. The cross marks the occurrence of a Type I X-ray burst, whereas open circles are nondetections. The arrow identifies the time of the *Chandra* observation.

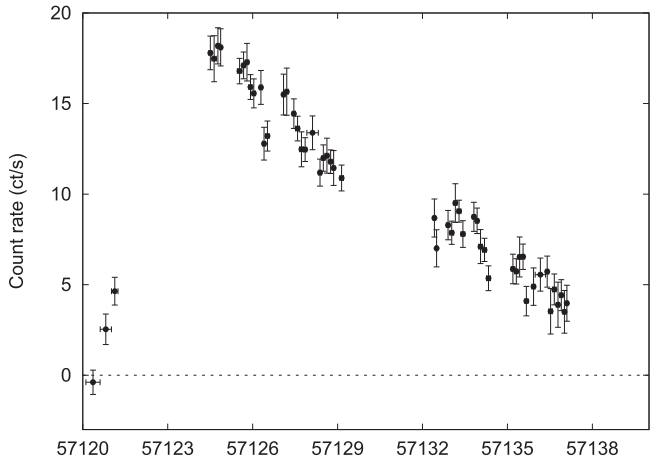

Figure 2. *INTEGRAL* IBIS light curve of the 2015 outburst in the 20–100 keV energy band. The onset of the outburst is detected around MJD 57121. The data points have typical integration times of 1800–3600 s. The horizontal error bars (larger than the symbols for only a few points) define the time interval over which the data has been integrated.

folding the data in stretches of ∼2000 s in pulse profiles composed by 32 bins.

The folding procedure used the ephemeris reported in Patruno et al. (2012) and extrapolated the solution to the time of the *Chandra* observation. Given the low signal-to-noise ratio (S/N) of the observations, we only measured the times of arrival (TOAs) of the fundamental pulse frequency (ν). This procedure to obtain the pulse TOAs is robust against a possible pulse shape variability (see Hartman et al. 2008 and Patruno et al. 2010 for details). To follow the evolution of the orbit and the pulsar spin, we fit the TOAs with the TEMPO2 (Hobbs et al. 2006) software, and, after obtaining a new best-fit ephemeris, we refolded the data (to obtain a higher S/N for the pulsations) and repeated the procedure. We stopped once the S/N of the pulsations did not increase any further.

We also created power-density spectra of the *Chandra* data. No background subtraction was applied to the data before calculating the power spectra. The Poissonian noise level was measured by taking the average power between 3000 and 4000 Hz, a region dominated by counting statistics noise alone. After obtaining the mean Poissonian value, we subtracted it from the power spectra.

We used 128 s segments to calculate the power spectra so that our frequency boundaries were 1/128 and 4096 Hz. The powers were normalized in the rms normalization (van der Klis 1995), which gives the power density in units of (rms/mean)^2 Hz^{-1}. We defined the fractional rms amplitude between the frequencies ν_1 and ν_2 as

$$\mathrm{rms} = \left[\int_{\nu_1}^{\nu_2} P(\nu) d\nu\right]^{1/2} \quad (1)$$

and calculated the errors from the dispersion of the data points in the power spectra.

3. Radio Observations

SAX J1808.4−3658 was observed on two different occasions, 2014 August 9 and 22 (MJD 56878 and MJD 56891, respectively), using the 110 m Robert C. Byrd GBT in West Virginia. During this period, it was known to be in X-ray quiescence, with the previous outburst having ended in 2011 and the next outburst starting in 2015 April. The data were recorded using the Green Bank Ultimate Pulsar Processing Instrument (GUPPI; DuPlain et al. 2008) backend. This combination of the GBT with GUPPI provides a high sensitivity to faint millisecond radio pulsations—arguably the deepest search that can be done with current radio telescopes, given that the source is well outside the Arecibo-visible declination range.

The distance to the source (3.5 kpc) suggests a relatively high expected dispersion measure (DM $\gtrsim$ 100 pc cm^{-3}, based

Table 1
GBT Summary of Observations

Obs. No.	Subint. No.	Obs. Start Date	Obs. Start MJD	Integration Time (minutes)	Orbital Phase Coverage
1	1	2014 Aug 09	56878.149456	16.1	0.97–0.10
1	2	2014 Aug 09	56878.160641	16.1	0.10–0.24
1	3	2014 Aug 09	56878.171826	16.1	0.24–0.37
1	4	2014 Aug 09	56878.183011	11.6	0.37–0.46
2	5	2014 Aug 22	56891.022211	16.1	0.39–0.53
2	6	2014 Aug 22	56891.033396	13.8	0.53–0.65

on the NE2001 model of Cordes & Lazio 2002, 2003). Furthermore, there is the potential for radio eclipses from intrabinary material in analogy with the rotation-powered BW and redback millisecond pulsar systems, where the eclipse duration is typically longer at lower radio frequencies, e.g., Stappers et al. (2001), and Archibald et al. (2013). Hence, our observations were conducted at a relatively high central observing frequency of 2 GHz in order to mitigate these effects while still maintaining sensitivity to the typically steep spectra of radio pulsars ($\nu^{-1.4}$, where ν is the frequency of the electromagnetic radiation; see Bates et al. 2013, although note that this result is specific to isolated nonrecycled pulsars). A previous and complementary search of SAX J1808.4−3658 used an even higher observing frequency of 5 GHz in order to avoid free–free absorption from eclipsing material, but it was correspondingly much less sensitive to steep-spectrum radio emission (Iacolina et al. 2010).

GUPPI provided 800 MHz of bandwidth, with 61.44 μs samples and 0.391 MHz frequency channels recorded as 8-bit samples in `psrfits` format. The orthogonal polarizations were summed in quadrature, providing only total intensity. We acquired 60 and 30 minute integrations on 2014 August 9 and 22, respectively. The observational setup and offline data analysis (see Section 4) were tested using the millisecond pulsar PSR J1824–2452A (M28A). In a blind periodicity and DM search, radio pulsations from M28A were easily recovered at the known pulsar spin frequency of 327.4 Hz and DM = 119.9 pc cm^{-1}.

4. Radio Data Analysis

We began the data analysis by sequentially combining groups of three observational subintegrations of 322 s each. This resulted in raw data sets of ∼16 minutes each (or slightly less if they were at the end of the observing session)—i.e., ∼13% of SAX J1808.4−3658's binary orbital period of 2.01 hr in each case. The total integration time was subdivided in this way in order to enable linear acceleration searches (see Section 4.1) and because of the potential for eclipsing, which, in analogy with the BW systems, could last for at least 10% of the orbit. The observation start times and duration and the corresponding orbital phases of SAX J1808.4−3658 are summarized in Table 1 (an orbital phase of 0.25 corresponds to superior conjunction of the neutron star).

Initial data preparation and periodicity searching were realized using `PRESTO`, a comprehensive pulsar processing software developed by Scott Ransom (for details, see Ransom 2001; Ransom et al. 2002, 2003). Radio frequency interference (RFI) was excised using an RFI mask generated with `rfifind`. Given that the DM toward SAX J1808.4−3658 is unknown, we used `prepsubband` to generate RFI-masked, barycentered, and dedispersed time series over trial DMs ranging from 0 to 1000 pc cm^{-3} (using a DM step size of 0.1 pc cm^{-3} up to a DM of 500 pc cm^{-3} and a step size of 0.3 pc cm^{-3} from 500 to 1000 pc cm^{-3}, resulting in a total of 6671 time series). For each time series, we created a corresponding Fourier power spectrum using `realfft`. The residual intra-channel DM smearing was 41–81 μs (i.e., 1.6%–3.2% of the pulse period) for DMs of 100–200 pc cm^{-3}, which corresponds to an approximate distance range of 3–6 kpc in the NE2001 model and should conservatively encompass the uncertainty on SAX J1808.4−3658's distance.

As described below, we searched the dedispersed time series for pulsations both by using a blind Fourier-based periodicity search and by directly folding the data using an X-ray–derived rotational and orbital ephemeris.

4.1. Blind Fourier-Based Periodicity Search

We first performed a blind periodicity search just in case the X-ray–derived ephemeris was inaccurate and to check the possibility of a serendipitous and unrelated radio pulsar along the line of sight.

The apparent rotational period of binary pulsars is Doppler shifted by their orbital motion. This results in a spreading of the spectral power over multiple Fourier bins as $z = aT^2/cP$, where z is the number of Fourier bins drifted, T is the integration length of the observation, c is the speed of light, and P is the spin period. For SAX J1808.4−3658, the maximum orbital acceleration is $a \approx 14\,\mathrm{m\,s^{-1}}$ (companion mass $M_c \sim 0.05$–$0.08\,M_\odot$), corresponding to a maximum drift of $z = 18$ bins in 16 minute observations. As demonstrated by Ransom et al. (2001, 2002), such a signal can be successfully recovered by searching over multiple linear frequency derivatives. We employed this technique of Fourier-based acceleration searches using `accelsearch` and searched $z_{\max} = 100$ for all 6671 Fourier power spectra (Section 4) in each ∼16 minute subintegration.

We then identified the best candidates from the above acceleration searches using the *ACCEL_sift* subroutine of `PRESTO`, which groups candidates found at different trial DMs. *ACCEL_sift* did not identify any candidates with a rotational period close to that of SAX J1808.4−3658. Nonetheless, in case there was a serendipitous pulsar along the same line of sight, for each of the *ACCEL_sift* candidates, we folded the corresponding dedispersed time series and selected those folds showing a reduced $\chi^2 > 2$ (this is used as a proxy for S/N in `PRESTO`) to also fold the raw data. We then inspected the candidates by eye and used parameters such as the shape and S/N of the cumulative pulse profile and the S/N as a function of DM from *prepfold* diagnostic output plots to make an informed selection. This inspection did not reveal any convincing pulsar candidates from the blind search.

4.2. Direct-Folding Search with X-Ray–Derived Ephemeris

With a priori knowledge of the spin and orbital parameters, it is possible to perform a deeper search for radio pulsations than the blind search discussed above. Previous coherent timing analysis of SAX J1808.4−3658, enabled by its X-ray pulsations during outbursts, provides such an ephemeris.

However, the short orbital period BW and redback millisecond pulsar binaries are known to show nondeterministic orbital variations (see Patruno et al. 2012; Archibald et al. 2013; Breton et al. 2013), and such variations should also be expected in the case of SAX J1808.4−3658, meaning that any previously derived ephemeris may not extrapolate well to future observations. X-ray pulsation searches in the redback transitional millisecond pulsar PSR J1023+0038 (e.g., Archibald et al. 2015; Jaodand et al. 2016) have established that one can successfully account for such nondeterministic orbital variations by searching over a small deviation in the time of ascending node ($T_{\rm asc}$). Therefore, when folding the GBT radio data with X-ray–derived ephemerides, we searched both over DM and a $\Delta T_{\rm asc}$ value compared to the fiducial ephemeris value.

Given the integration times of 1 and 0.5 hr during the first and second observation epochs, respectively, we could ensure significant orbital coverage of SAX J1808.4−3658's ∼2 hr orbit such that at least some observations were close to the inferior conjunction of the neutron star (see Table 1). We used two known orbital ephemerides: the one obtained from coherent timing analysis up to 2011 (Patruno et al. 2012) and the one obtained by also including the 2015 outburst (Section 4.2). In addition, we varied $T_{\rm asc}$ over a range of ±30 s in steps of 0.1 s, resulting in 2×600 trial ephemerides per DM trial.

Each of the 6671 dedispersed time series for every 16 minute subintegration were then folded using `prepfold` and the 2×600 ephemerides. Moreover, the folding operation was conducted in two additional ways: by allowing `prepfold` to optimize the S/N in a narrow range of spin period and spin-period derivative around the nominal ephemeris prediction and only allowing an optimization in spin-period derivative. Hence, at the end of these ephemeris-based searches, we obtained $2 \times 2 \times 6671 \times 600 = 16,010,400$ folded profiles. We filtered the profiles by creating histograms of the S/N of the folds in each 16 minute subintegration and choosing only candidates with reduced $\chi^2 \gtrsim 2$ to inspect by eye. We found no candidate profiles with sufficient S/N that clearly peaked in both trial DM and $\Delta T_{\rm asc}$. This procedure was also verified using our test pulsar observations of M28A.

5. Results

5.1. X-Ray Light Curve

SAX J1808.4−3658 was detected in outburst with the *Swift* Burst Alert Telescope (BAT) on 2015 April 9 (MJD 57121; Sanna et al. 2015). During the closest previous *Swift* XRT observation, which occurred on April 3 (MJD 57195), SAX J1808.4−3658 was still in quiescence (Campana et al. 2015). The 0.3–10 keV X-ray light curve of SAX J1808.4−3658 (see Figure 1) shows the very typical evolution that was also observed in the other outbursts. The outburst started approximately 3.5 yr after the previous one, in line with the typical recurrence time of 3–4 yr.

The *Swift* XRT started monitoring SAX J1808.4−3658 after a Type I X-ray burst on April 11 (MJD 57123). The source showed the same evolution seen in previous outbursts, with an observed 0.3–10 keV peak flux of $\approx 3 \times 10^{-9}$ erg s^{-1} cm^{-2} that (assuming a distance of 3.5 kpc; Galloway & Cumming 2006) corresponds to a luminosity of 4×10^{36} erg s^{-1}. The outburst showed an initial near-exponential decay (slow decay) lasting about 15 days. It then transitioned into a faster linear decay for about 5 days when the source reached a luminosity of $\approx 10^{35}$ erg s^{-1} before entering a prolonged outburst reflaring tail that lasted another ∼100 days.

During the outburst reflaring tail, typical of all previous outbursts (van der Klis 2000; Wijnands et al. 2001, 2003; Campana et al. 2008; Patruno et al. 2009c, 2016), the luminosity of the source oscillated between very faint states close to 2×10^{32} erg s^{-1} and relatively brighter ones of $\sim 10^{36}$ erg s^{-1}. Two bright reflares were seen in 2015, on May 13 (MJD 57155) and May 18 (MJD 57164), after which several progressively weaker reflares followed on a cadence of 5–10 days. The *Chandra* observation we report in this work took place during the second bright reflare.

The power spectra of the *Chandra* data show no relevant feature at any frequency. We exclude the presence of a 1 Hz modulation (similar to that observed in several previous outbursts) with an rms amplitude larger than 10% at the 95% confidence level. This upper limit is derived by looking at the power in the 0.05–10 Hz range, as in, e.g., Patruno et al. (2009c).

5.2. X-Ray Pulsations

The X-ray pulsations are very clearly detected in each data segment at the 4σ–8σ level, where we define the significance as the ratio between the pulse amplitude and its statistical error. The sinusoidal fractional amplitude of the pulsations is, on average, around 2% (sinusoidal amplitude or semi-amplitude) and does not show any significant variation during the duration of the observations. The pulse TOAs are fitted with a constant pulse frequency plus a Keplerian circular orbit, and the statistical errors on the fitted parameters are obtained with standard χ^2 minimization techniques.

Since we do not see any significant timing noise in the data (at the timescales of the observations) and the variance of the pulse TOAs is compatible with that expected from measurement errors alone, we take our statistical errors as a good representation of the true statistical ones. In previous work (e.g., Hartman et al. 2008; Patruno et al. 2012), it was shown that, when observing the pulsations of SAX J1808.4−3658, a strong timing noise is always observed on timescales of the order of hours to days. Part of this noise is correlated to X-ray flux variations and introduces systematic errors on the determination of the spin frequency of the order of 10^{-8}–10^{-7} Hz. These systematic errors are particularly pronounced during the reflares, when strong pulse shape variability is observed (Hartman et al. 2008, 2009). The magnitude of such systematic errors can be estimated by looking at data stretches that are longer than the typical timing noise timescales. However, since the pulsations available in our analysis refer only to a short data span (≈30 ks), we cannot determine the size of the systematic errors in our analysis. Indeed, Hartman et al. (2008, 2009) and Patruno et al. (2012) estimated the average systematic error on the pulse frequency over the entire baseline of the observations, which lasted for weeks/months. Here, instead, the much shorter data span implies that the systematic effect of timing noise can be substantially larger

Table 2
SAX J1808.4−3658 Timing Solution for the 2015 Outburst

Parameter	Value	Stat. Error	Syst. Error
ν (Hz)	400.9752067	1.1×10^{-6}	$\sim 10^{-6}$
$T_{\rm asc}$ (MJD)	57167.025002	7×10^{-6}	...
e	<0.003	(95% c.l.)	...
$a_1 \sin i$[a] (lt-ms)	62.812	2×10^{-3}	...
P_b[a] (s)	7249.156980	4×10^{-6}	...
Eccentricity e[a] (95% c.l.)	$<1.2 \times 10^{-4}$	...	...
Epoch (MJD)	52499.9602472	...	...

Note.
[a] These values are taken from Hartman et al. (2009) and are kept fixed during the fit.

than average. For example, by looking at Figure 1 in Hartman et al. (2009), we see that on timescales of a few hours the timing noise can induce pulse phase shifts on the order of 0.1–0.3 cycles. For this work, such a phase shift would translate into systematic errors on the determination of the pulse frequency of up to a few 10^{-6} Hz.

Even if our statistical errors on the pulse frequency are large ($\sim 10^{-6}$ Hz), we cannot neglect the effect of systematic errors, although we can only use a rough estimate of the magnitude by looking at the behavior of the pulsations recorded during previous outbursts. The orbital and pulse frequency solution is reported in Table 2.

5.3. Orbital Solution

To determine the orbital evolution, we follow the procedure used in Patruno et al. (2012) and Hartman et al. (2008, 2009) and fit the time of passage through the ascending node (which is equivalent to orbital phase zero) together with the measurements of the previous outbursts. The reference point $T_{\rm asc,ref}$ is taken from Table 1 of Hartman et al. (2009), and we use the quantity $\Delta T_{\rm asc} = T_{\rm asc,i} - (T_{\rm asc,ref} + N\,P_b)$, where $T_{\rm asc,i}$ refers to the ith outburst and N is the closest integer to $(T_{\rm asc,i} - T_{\rm asc,ref})/P_b$. The reference orbital period P_b can also be found in Table 1 of Hartman et al. (2009).

Up to the 2008 outburst, the $\Delta T_{\rm asc}$ evolution showed a trend that was compatible with a quadratic polynomial representing an orbital expansion at a constant rate (di Salvo et al. 2008; Hartman et al. 2008). Indeed, the time of passage through the ascending node can be expressed as a polynomial expansion:

$$T_{\rm asc}(N) = T_{\rm asc,ref} + P_b N + \frac{1}{2} P_b \dot{P}_b N^2 + \ldots . \quad (2)$$

By adding the 2011 outburst data points, Patruno et al. (2012) showed that a quadratic polynomial was insufficient to describe the observed behavior of the $T_{\rm asc}$ variations, which were instead successfully described by a cubic polynomial. The physical interpretation given was that, on the observed baseline of 13 yr, the orbit was expanding at an accelerated rate.

We now add the 2015 outburst data (see Figure 3), and we first try to fit the $T_{\rm asc}$ data points with a quadratic polynomial, which corresponds to the solution found in Hartman et al. (2008, 2009) and di Salvo et al. (2008). The fit is statistically poor, with a χ^2 of 492 for 4 degrees of freedom (dof). A cubic polynomial is also a poor description of the data, with $\chi^2/{\rm dof} = 314/3$. To obtain a p-value above the canonical 5% threshold, we need to fit the data with a fifth-order polynomial ($\chi^2/{\rm dof} = 3.4/1$, p-value 6%), which suggests that either the observed variability is governed by a stochastic process or, if a periodicity is present, it must be significantly longer than the observational baseline.[11] The concavity of the fifth-order polynomial curve changes sign around 2011, which implies that the orbit started to shrink after that time.

Next, we try to fit the data with a sinusoid that could represent the effect of a slightly eccentric orbit with periastron advance. From our previous work (Patruno et al. 2012), we already know that a sinusoid is a statistically poor fit to the data. Indeed, we find a formally bad fit with a $\chi^2 = 83.9$ for 2 dof. Furthermore, the fit requires an eccentricity of about 0.004, which is much larger than the best upper limits available on SAX J1808.4−3658 ($e < 1.2 \times 10^{-4}$; Hartman et al. 2009). Finally, we attempt to fit the data with a Keplerian orbital delay curve that could represent the effect of orbital motion caused by a third body in an eccentric orbit. We find that this can fit the data (with $\chi^2 = 1.1$ for 1 dof) if the third body has a mass of about 8 Jupiter masses and is in a relatively wide (≈5 au) orbit with an eccentricity of about 0.7 and an orbital period of about 17.4 yr. We can test this scenario by looking at the pulse frequency derivative of SAX J1808.4−3658, since the pulsar would be accelerated along the orbit. Given the fitted orbital parameters, the orbital velocity would be $v_{\rm orb} \approx 50\,{\rm m\,s^{-1}}$, with variations along the orbit due to the large eccentricity. To get a first-order orbital acceleration, we use $e = 0$ and get $a_{\rm orb} \approx 6 \times 10^{-7}\,{\rm m\,s^{-2}}$. This would imply a pulse frequency derivative of (Joshi & Rasio 1997)

$$\dot{\nu}_p = \nu_s \frac{\boldsymbol{a}_{\rm orb} \cdot \boldsymbol{n}}{c}, \quad (3)$$

where $\boldsymbol{n}$ is a unit vector along the line of sight and $\nu_s = 401$ Hz is the spin frequency of SAX J1808.4−3658. This gives $\dot{\nu}_p = 8 \times 10^{-13} \cos\theta$, where θ is the angle between the acceleration and line-of-sight vectors. Since we know from previous observations that SAX J1808.4−3658 is spinning down at a relatively constant rate of $\dot{\nu}_s \approx 10^{-15}\,{\rm Hz\,s^{-1}}$, we can confidently exclude this scenario.

5.4. Radio Pulse Search

Exhaustive searches using a blind Fourier-based periodicity search and folding with a range of perturbed ephemerides failed to find radio pulsations from SAX J1808.4−3658 for any trial DM or $\Delta T_{\rm asc}$ (see Section 4).

In the absence of detectable radio pulsations, we can place a stringent upper limit on pulsed radio emission from SAX J1808.4−3658, with the notable caveat that an active radio pulsar could, in principle, be enshrouded by intra-binary material for a large fraction of the time (e.g., Archibald et al. 2013). In analogy with the BW systems, however, it is reasonable to assume that SAX J1808.4−3658 would only be eclipsed for ∼10% of its orbit at a 2 GHz observing frequency.

To set an upper limit on the flux density, we use the modified radiometer equation (see Dewey et al. 1985; Bhattacharya 1998;

[11] As a cautionary test, we also try to remove the 2011 point (assuming it is an outlier, even if there is no evidence or reason to believe that this is the case) and fit the data again with a quadratic polynomial. The data also give a poor fit, with $\chi^2 = 11.1$ for 3 dof (and p-value ≈1%).

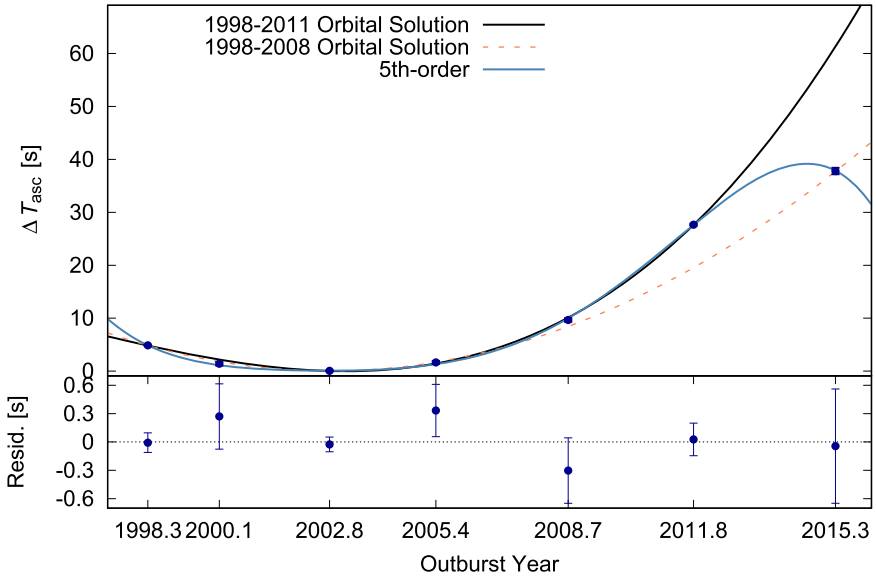

Figure 3. Orbital evolution of SAX J1808.4−3658 over 17 yr. The $\Delta T_{\rm asc}$ cannot be fitted with a cubic (solid black line) or quadratic (dotted orange line) polynomial. A fifth-order polynomial (solid blue line) is necessary to obtain a statistically acceptable fit, which suggests a complex behavior of the orbit. The panel at the bottom shows the residuals with respect to the fifth-order polynomial fit.

Lorimer & Kramer 2012):

$$S_{\rm min} = \frac{\left(\frac{\rm S}{\rm N}\right)\beta\,(T_{\rm sys}+T_{\rm sky})}{G\,\sqrt{n_p\,t_{\rm obs}\,\triangle\nu}}\,\sqrt{\frac{W}{P-W}}. \quad (4)$$

We use the S-band receiver/frontend (Rcvr2_3) at the GBT. For this receiver, the system noise temperature $T_{\rm sys}$ is 22 K, and the gain of the telescope G is 1.9 K Jy^{-1}. The sky temperature, $T_{\rm sky}$, is ∼3 K. Here, $\triangle\nu$ is the 800 MHz bandwidth, the correction factor β is assumed ideal and close to 1, the number of polarizations n_p is two, and the integration time $t_{\rm obs}$ corresponds to 16 minutes.[12] With the assumption that the pulse duty cycle is ∼10% and the $\rm S/N\left(\frac{S}{N}\right)_{min}$ for candidate identification by eye is 8, we obtain a maximum flux density for SAX J1808.4−3658 of 30 μJy at 2 GHz (equivalently, 50 μJy at 1.4 GHz, for an assumed spectral index of $\alpha=-1.4$).

This limit can be used as an important input for future radio searches and a point of comparison in the event that SAX J1808.4−3658 becomes a detectable radio pulsar in the future. We note that, of the 116 Galactic field millisecond pulsars with spin periods less than 10 ms (see Australia Telescope National Facility (ATNF) pulsar catalog, version 1.56, at http://www.atnf.csiro.au/research/pulsar/psrcat/; see also Manchester et al. 2005) with quoted flux densities at 1.4 GHz, less than 10% have an average flux density smaller than the upper limit we set on SAX J1808.4−3658. For an assumed distance of 3.5 kpc, the implied pseudo-luminosity limit is $L_1400 = 50\ \mu{\rm Jy}\times(d/d_{3.5\,{\rm kpc}})^2 = 0.6$ mJy kpc^2, which is in the lowest 25% compared to the known millisecond pulsar population.

[12] While we could, in principle, quote a 2× deeper limit by coherently folding the full 1 hr 2014 August 9 data set, we choose not to do so because some fraction of this integration is during orbital phases in which any radio pulsar is likely to be eclipsed. We therefore prefer to set a more conservative flux density limit using the 16 minute subintegrations, which together span a wide range of orbital phases.

6. Discussion

We have conducted the deepest radio pulse search of SAX J1808.4−3658 during its quiescent phase in 2014 August. No radio pulsations have been detected, setting the strongest possible upper limit (30 μJy at 2 GHz) on the presence of radio pulsations that exist (to date) for any AMXP. Iacolina et al. (2010) performed radio pulsation searches toward SAX J1808.4–3658 at the higher observing frequency of 5 GHz and obtained an upper limit of 59 μJy on the presence of radio pulsations (this is equivalent to a 2 GHz upper limit of 280 μJy, if one assumes a power-law spectrum with index −1.7). Their approach assumed that detectability would be limited by free–free absorption, which could be avoided by observing at higher frequencies. In the present work, we assume that 2 GHz is a sufficiently high frequency that the putative radio pulsar is sometimes visible out of eclipse. The advantage of observing at lower frequencies is that the radio spectrum is likely to be steep.

The presence of a radio pulsar turning on during quiescence cannot be excluded with the present upper limits. However, if a radio pulsar signal is present, it has to be quite weak (weaker than the majority of known radio millisecond pulsars; see Section 5.4), substantially scattered by the intervening interstellar medium, or perpetually eclipsed in order to remain compatible with the current constraints. The beam width of millisecond radio pulsars is very large (typical values of ∼100°; e.g., Lorimer 2008) so that missing the pulsar because of beaming, although possible, is unlikely. The strongest evidence for a large beaming angle comes from X-ray observations of globular clusters, where very few unidentified X-ray sources have spectral properties compatible with unknown millisecond pulsars whose radio beams are not pointing toward Earth (Heinke et al. 2005). Even if SAX J1808.4−3658 is an active radio pulsar in quiescence, there is still a good chance that eclipses might appear for 10%–50% of the orbit due to free–free absorption by intra-binary material, a common occurrence in BW and redback pulsars (Nice et al. 2000; Roberts 2013). To avoid this problem, we have

observed at a high-enough radio frequency that a long eclipse duration is unlikely. We have also observed at a wide range of orbital phases, when the neutron star is not behind its companion.

After 17 yr of X-ray monitoring, the orbital period evolution of SAX J1808.4−3658 shows a nonpredictable behavior. The statistical fit to the data shows that neither a parabolic nor a cubic polynomial can describe the data correctly. We find an ambiguity in the interpretation of the long-term trend of $T_{\rm asc}$, since the observations can be explained in two ways. Either the orbit is expanding throughout the 17 yr observational window, with some fluctuations around the mean $\dot{P}_b$, or it expanded until ∼2011, followed by a shrinkage (i.e., the fifth-order polynomial curve changes concavity). This is not a surprising behavior, since many binary systems have shown a similar orbital evolution. However, identifying the precise short-term mechanism responsible for such orbital evolution is a relatively difficult task.

In the following, we first discuss some fundamental properties of binary evolution; we then compare SAX J1808.4−3658 to other known binaries that show anomalous orbital evolution. Finally, we review possible mechanisms to explain such an anomaly.

6.1. Binary Evolution Timescales

Looking at the binary evolution, it is useful to define a timescale $\tau_{\rm ev} = \frac{P_b}{\dot{P}_b}$ that can be compared to the expected evolutionary timescales from theoretical models. Differentiating the third Kepler law and assuming that all mass lost by the companion is accreted by the primary, one obtains the well-known equation (see, e.g., Frank et al. 2002)

$$\frac{\dot{a}}{a} = \frac{2\dot{J}}{J} + \frac{-2\dot{M}_{\rm c}}{M_{\rm c}}(1-q), \tag{5}$$

where $q = M_{\rm c}/M_{\rm NS}$ is the mass ratio between the companion ($M_{\rm c}$) and the neutron star mass ($M_{\rm NS}$), a is the orbital separation, J is the angular momentum, and the dot refers to the first time derivative. In general, the angular momentum loss of the binary ($\dot{J}$) can be decomposed in four terms (see, e.g., Tauris & van den Heuvel 2006),

$$\frac{\dot{J}}{J} = \frac{\dot{J}_{\rm gw}}{J} + \frac{\dot{J}_{\rm mb}}{J} + \frac{\dot{J}_{\rm ml}}{J} + \frac{\dot{J}_{\rm soc}}{J}, \tag{6}$$

where the subscripts gw, mb, ml, and soc refer to gravitational-wave emission, magnetic braking, mass loss, and spin–orbit coupling, respectively. When the binary is relatively compact (orbital period of less than ∼1 day), the evolution of the system is believed to be driven by angular momentum loss (encoded in the $\dot{J}$ term in the expression above; see, e.g., Frank et al. 2002) rather than the nuclear evolution of the donor star. In ultra-compact ($P_b < 80$ minutes) and compact (80 minutes $< P_b \lesssim 3.5$ hr) binaries, the angular momentum loss is believed to be mainly due to emission of gravitational waves ($\dot{J}_{\rm gw}$), which becomes very efficient at short orbital separations (van der Sluys 2011). If there is no mass loss from the system, then the loss of angular momentum via gravitational waves drives the mass transfer and the orbital period changes according to the following expression (Rappaport et al. 1987; Verbunt 1993; di Salvo et al. 2008):

$$\dot{P}_b = -1.4 \times 10^{-14} M_{\rm NS} M_{\rm c} M^{-1/3} P_{\rm b,hr}^{-5/3} \times (\zeta - 1/3)/(\zeta + 5/3 - 2q), \tag{7}$$

where all masses are expressed in solar units, $P_{\rm b,hr}$ is the orbital period in hours, and ζ is the effective mass–radius index of the donor star ($R_{\rm c} \propto M_{\rm c}^{\zeta}$; see, e.g., van Teeseling & King 1998).

When the orbital period of the binary is wider, in the range of 3.5 hr $\lesssim P_b \lesssim$ 0.5–1 day, the dominant mechanism driving the binary evolution is thought to be angular momentum loss via magnetic braking ($\dot{J}_{\rm mb}$). There is currently considerable uncertainty about the details of magnetic braking because its efficiency depends on a number of poorly understood (and difficult to measure) stellar parameters (see, e.g., Knigge et al. 2011 for a discussion). It also remains rather speculative whether the single-star braking laws can be extended, unaltered, to binary systems. Given these uncertainties, the magnetic-braking timescale can vary by up to an order of magnitude, and, indeed, different recipes have been given in the literature (Skumanich 1972; Rappaport et al. 1983; Stepien 1995; see also Tauris & van den Heuvel 2006 and Appendix A in Knigge et al. 2011 for a review of several magnetic-braking models). Nonetheless, moderately wide binaries where magnetic braking is dominant are thought to lose angular momentum on shorter timescales than those compact binaries where angular momentum loss is dominated by gravitational-wave emission. The orbital parameters of SAX J1808.4−3658 imply that it is a binary whose evolution should be determined by gravitational-wave emission alone, since magnetic braking is believed to turn off (or become less efficient) once the donor becomes fully convective and/or semi-degenerate (Spruit & Ritter 1983; see, however, Wright & Drake 2016 for recent results that suggest that a dynamo process might still occur in fully convective stars).

It is interesting at this point to compare what is observed in compact radio pulsar binaries (BWs and redbacks; see, e.g., Roberts 2013), as well as other LMXBs and accreting white dwarfs that have orbital parameters similar to those of SAX J1808.4−3658 and have a measured $\dot{P}_b$. The reason these systems might be relevant in this context is twofold: other LMXBs might be behaving similarly to SAX J1808.4−3658, since the same mechanisms might be at play, whereas BWs and redbacks are nonaccreting systems, and therefore Equation (5) simplifies. In the last few years, three redback pulsars have transitioned to an accreting LMXB state (Archibald et al. 2009; Papitto et al. 2013; Bassa et al. 2014; Roy et al. 2015). Therefore, it is still possible that more of these systems (if not all) could display the same behavior, and the assumption that redbacks are always nonaccreting might be invalid. As yet, no BW system has been observed to transition from a rotation-powered to an accretion-powered state.

6.2. Comparison with Other Interacting Binaries

Among the binary pulsars, we discuss below only the cases of the BWs and redbacks, because all binaries with a white dwarf/neutron star companion are following the predictions of general relativity with exquisite precision (e.g., Taylor & Weisberg 1989; Weisberg & Taylor 2002). We also exclude from the sample those radio pulsars with a B-type star companion, since very different mechanisms involving the short nuclear evolution timescale of the massive companion

Table 3
BWs and Redbacks with Measured $\dot{P}_b$

Name (PSR)	Type	P_b (hr)	$\dot{P}_b$	Error
J1023+0038	RB	4.8	-7.3×10^{-11}	0.06×10^{-11}
J1227−4853	RB	6.9	-8.7×10^{-10}	0.1×10^{-10}
J1723−2837	RB	14.8	-3.5×10^{-9}	0.12×10^{-9}
J2339−0533[a]	RB	4.6	$[-5.8, 2.7] \times 10^{-10}$	0.01×10^{-10}
J1731−1847	BW	7.5	-1.08×10^{10}	0.07×10^{-10}
J2051−0827[a]	BW	2.4	$[-2.03, 1.41] \times 10^{-11}$	0.08×10^{-11}
J1959+2048	BW	9.2	1.47×10^{-11}	0.08×10^{-11}

Note.
[a] The orbital period of these pulsars shows a roughly cyclic behavior; see Shaifullah et al. (2016) and Pletsch & Clark (2015).

need to be considered. This is also the reason that we do not include high-mass X-ray binaries in our sample.

6.2.1. BWs and Redbacks

In BWs and redbacks, the companion star is being ablated by the pulsar wind and high-energy radiation, thus producing potential mass loss. Observational evidence of this phenomenon comes from the fact that radio pulsations are very often eclipsed by intra-binary material that induces free–free absorption of the pulsed signal. The orbital parameters of SAX J1808.4−3658 are compatible with those of a BW, and its 0.05–0.08 $M_\odot$ companion is also a semi-degenerate star (Bildsten & Chakrabarty 2001; Deloye et al. 2008; Wang et al. 2013). The only difference between BWs and SAX J1808.4−3658 is that, in the latter system, the companion is in Roche lobe overflow, whereas BWs are thought (at least in some cases) to be detached systems (Breton et al. 2013).

In BWs, as well as in redback pulsars, short-term effects on the orbital evolution occur on timescales that are generally orders of magnitude shorter than the predicted (secular) ones from angular momentum loss due to gravitational waves and/or magnetic braking. The seven BWs and redbacks that have a measured $\dot{P}_b$ show orbital evolution timescales from 100 Myr to less than 1 Myr (see Table 3). Four of them have a negative orbital period derivative (the orbit is shrinking), whereas only one (PSR J1959+2048) has a positive value (the orbit is expanding). In at least two cases (PSR J2051–0827 and PSR J2339–0533), the sign seems to be changing cyclically over timescales of the order of a few years (Pletsch & Clark 2015; Shaifullah et al. 2016).

Similarly, in the case of SAX J1808.4−3658, $\tau_{\rm ev} = \frac{P_b}{\dot{P}_b} \approx$ 70 Myr, whereas from Equation (7) one would have expected a timescale of a few Gyr (varying slightly with the exact neutron star and companion mass chosen), meaning that the $\dot{J}_{\rm gw}$ term is not the dominant one. It is important to stress that these apparent orbital period derivatives are epoch-dependent in all BWs and redbacks and change on years-long timescales. However, there is at least one situation where, besides the short-term fluctuations discussed above, there is also a decade-long (secular?) variation of the orbit that corresponds to an overall shrinkage of the binary orbital separation (see, e.g., PSR J1023+0038; Jaodand et al. 2016).

6.2.2. Other LMXBs

In the few compact LMXBs where an orbital period derivative can be measured, we see a roughly equally distributed sign (six positive and four negative signs and three upper limits observed so far; see Table 4). The magnitude of the orbital period derivative is always much larger than expected from conservative binary evolution ($\dot{J} = 0$) and/or from angular momentum loss via gravitational waves and/or magnetic braking. In the literature, a number of different mechanisms have been suggested to explain the large $\dot{P}_b$. These include mass loss from the companion (Burderi et al. 2010; Ponti et al. 2017), enhanced magnetic braking (González Hernández et al. 2014), the presence of a third body (Iaria et al. 2015), spin–orbit coupling (Wolff et al. 2009; Patruno et al. 2012), and, in some cases, even modified theories of gravity (Yagi 2012). The group of LMXBs appears to be the most heterogeneous among the different binaries that we are considering here. Indeed, this group comprises transient LMXBs with black hole accretors (XTE J1118+480 and A0620–00), transient LMXBs with neutron star accretors (EXO 0748–676, MXB 1658–298, SAX J1748.9–2021, AX J1745.6–2901, and SAX J1808.4−3658), and persistent neutron star LMXBs (Her X–1, 2A 1822–37, and XB 1916–053). Furthermore, some of these LMXBs are accreting pulsars and have orbital periods determined via timing of their pulsations (e.g., Her X–1, 2A 1822–37, SAX J1808.4−3658, and SAX J1748.9–2021), whereas others are eclipsing systems and their periods are determined via X-ray and/or optical photometry. No other orbital period derivative has been measured so far for any other LMXB. In Table 4, we list the LMXBs in the sample with their orbital period derivatives and the main proposed explanation given in the literature.

The binary EXO 0748–676 is an eclipsing binary with a 0.4 $M_\odot$ donor that shows sudden variations in $\dot{P}_b$, which were proposed to be due to spin–orbit coupling (Wolff et al. 2002, 2009). Wolff et al. (2002) analyzed two segments of X-ray data (1985–1990 and 1996–2000) and showed that the period had increased by about 8 ms. However, the period increase shows jitters and cannot be fit with a constant $\dot{P}_b$. Further work by Wolff et al. (2009) extended the analysis until 2008 and observed a similar behavior.

The eclipsing binary 2A 1822–37 is an accreting pulsar with an ∼0.3–0.4 $M_\odot$ companion, and it has a relatively steady increase of the orbital period measured over a baseline of 30 yr (see, e.g., Burderi et al. 2010; Iaria et al. 2011; Chou et al. 2016). This system is an accretion-disk corona system showing extended partial eclipses of the central X-ray source. Burderi et al. (2010) and Iaria et al. (2011) suggested that the binary contains an Eddington-limited accreting neutron star whose irradiation of the donor is inducing severe mass loss that can explain the large orbital period derivative observed. The positive sign of $\dot{P}_b$ is ascribed to the response of the radius of the donor to mass loss, with $R_{\rm c} \propto M_{\rm c}^{\zeta}$ and $n < 1/3$. Burderi et al. (2010) suggested that the donor in 2A 1822–37 has a deep convective envelope with $\zeta = -1/3$ (see, e.g., Rappaport et al. 1982), thus justifying the positive $\dot{P}_b$.

The source AX J1745.6–2901 is an eclipsing binary with an accreting neutron star and a negative $\dot{P}_b$ (Ponti et al. 2017). The donor mass is constrained to be $M_{\rm c} \lesssim 0.8\,M_\odot$. A strong mass loss is also suggested in this case; but, since the system is shrinking, the mass–radius index needs to be $n > 1/3$. The data on the $T_{\rm asc}$ collected over a baseline of about 30 yr show significant scatter of up to several tens of seconds.

The source XB 1916–053 is an ultra-compact ($P_b \approx$ 50 minutes) persistent dipping source monitored for over 37 yr by

Table 4
LMXBs with Orbital Period Derivatives

Name	P_b (hr)	$\dot{P}_b$	Transient	Companion Type	Sign	Proposed Model	References
Neutron Star LMXBs							
EXO 0748–676[a]	3.8	1.9×10^{-11}	Yes	MS	+	SOC	Wolff et al. (2002, 2009)
2A 1822–37	5.5	$1.51(8) \times 10^{-10}$	No	MS	+	Mass Loss	Burderi et al. (2010), Iaria et al. (2011)
SAX J1808.4–3658	2.0	$3.5(2) \times 10^{-12}$	Yes	SD	+	SOC/Mass Loss	di Salvo et al. (2008),Patruno et al. (2012)
MXB 1658–298	7.1	$8.4(9) \times 10^{-12}$	Yes	MS	+	Unknown	Paul & Jain (2010)
XB 1916–053	0.8	$1.5(3) \times 10^{-11}$	No	SD	+	Third Body	Iaria et al. (2015)
SAX J1748.9–2021	8.8	$1.1(3) \times 10^{-10}$	Yes	MS/Sub-G	+	Mass Loss	Sanna et al. (2016)
AX J1745.6–2901	8.4	$-4.03(32) \times 10^{-11}$	Yes	MS/Sub-G	−	Mass Loss	Ponti et al. (2017)
Hercules X–1	40.8	$-4.85(13) \times 10^{-11}$	No	MS	−	Several	Staubert et al. (2009)
XTE J1710–281[b]	3.2	$[-1.6, 0.2] \times 10^{-12}$	Yes	MS	UL	...	Jain & Paul (2011)
IGR J00291+5934[c]	2.5	$[-5, 6] \times 10^{-12}$	Yes	SD	UL	...	Patruno (2016)
4U 1323–619[d]	2.9	$[-5, 21] \times 10^{-12}$	No	MS	UL	...	Gambino et al. (2016)
Black Hole LMXBs							
XTE J1118+480	4.0	$-6(1.8) \times 10^{-11}$	Yes	MS	−	Enhanced MB	González Hernández et al. (2012, 2014)
A0620–00	7.8	$-1.9(3) \times 10^{-11}$	Yes	MS	−	Enhanced MB	González Hernández et al. (2014)
Nova Muscae 1991	10.4	$-6(4) \times 10^{-10}$	Yes	MS	−	Enhanced MB	González Hernández et al. (2017)

Notes. UL—upper limits; MS—main sequence; Sub-G—sub-giant; SD—semi-degenerate; MB—magnetic braking; SOC—spin–orbit coupling.
[a] This source shows segments of data where a constant P_b is required. The error on $\dot{P}_b$ is not given, and confidence intervals are determined via the maximum likelihood method (Wolff et al. 2009).
[b] 1σ upper limit.
[c] 90% confidence level upper limit.
[d] 1σ upper limit.

X-ray satellites. Hu et al. (2008) studied the first 24 yr of data and found that a quadratic function (i.e., a constant $\dot{P}_b$) was able to describe the data correctly. However, Iaria et al. (2015) found that, when considering the entire 37 yr of observations, a quadratic function was unable to fit the orbital evolution, and a model with a sinusoidal variation in addition to the quadratic component was required. A third body with a mass of $\sim 0.06\,M_\odot$ was invoked to explain the observations with an orbital period of $\approx$26 yr. It is instructive to note that a deviation from a quadratic function was not apparent in the first 24 yr of data, which suggests that a very long timescale periodicity (or quasi-periodicity) might still be present even in binaries where a constant $\dot{P}_b$ is observed over baselines of a few decades.

The globular cluster source SAX J1748.9–2021 is an intermittent AMXP (Gavriil et al. 2007; Altamirano et al. 2008; Patruno et al. 2009a; Sanna et al. 2016), and it has been observed in outburst five times. Its companion star is likely to be an $\sim 0.8\,M_\odot$ star close to the turnoff mass of the globular cluster NGC 6440, although much smaller masses down to $0.1\,M_\odot$ cannot be excluded (Altamirano et al. 2008). The orbital evolution has been studied by looking at the orbital ephemeris calculated with coherent timing in a way similar to what has been done in this work. Sanna et al. (2016) described the orbital evolution with a quadratic function, although the fit shows large deviations of the order of 100 s from the best-fit function (which translates into a poor χ^2 of 78.4 for 1 dof). These authors interpreted the large orbital expansion with a highly nonconservative mass-loss scenario in which the binary is losing more than 97% of the mass flowing through the inner Lagrangian point L_1.

Her X–1 shows a steady decrease of the orbit whose value is compatible with both a conservative and a nonconservative mass transfer scenario (Staubert et al. 2009).

Finally, the orbital evolution of the transient black hole LMXBs XTE J1118+480 and A0620–00 (González Hernández et al. 2012, 2014) was measured with radial velocity curves determined via optical spectroscopy for a period of $\sim$10 and 20 yr, respectively. These observations were carried out during the extended periods of quiescence of the binaries. The orbit shows a steady shrinkage interpreted as being due to enhanced magnetic braking. The two binaries have a companion mass of $0.2\,M_\odot$ (XTE J1118+480; González Hernández et al. 2014) and $0.4\,M_\odot$ (A0620–00; Cantrell et al. 2010; González Hernández et al. 2014).

6.2.3. Cataclysmic Variables

It is well known that some cataclysmic variables show an anomalous orbital period derivative as well, with some of them proposed to be transferring mass at a higher rate than expected due to irradiation of the companion (Knigge et al. 2000; Patterson et al. 2015, 2016). Even some Algol-type binaries (i.e., a semi-detached system composed of a detached early-type main-sequence star and a less massive subgiant/giant star in Roche lobe overflow) have been reported to evolve on a very short timescale (Erdem & Öztürk 2014). In this case, a nonconservative mass transfer scenario is expected to take place, since the red giant will emit a significant wind. However, for a few of these systems (i.e., all the converging ones), the required mass loss is larger than the highest theoretical value for wind mass loss in giant stars. These observations might suggest that short-term effects have some influence on the orbital evolution of accreting and nonaccreting neutron stars, persistent and transient systems, and white dwarf/black hole/main-sequence stellar accretors. It is worth noting that no neutron star + white dwarf binary (both accreting and nonaccreting) has been observed (as yet) to evolve on

anomalous timescales. The only exception is the ultra-compact LMXB 4U 1822–30, which, however, is located in a globular cluster, and therefore its large $\dot{P}_b$ might simply be due to the contamination induced by the gravitational potential well of the cluster (Jain et al. 2010; Perera et al. 2017). This suggests that, if there is a common reason behind this behavior for all types of binaries (which is, of course, not necessarily true), it must be related to the type of companion (main-sequence or semi-degenerate star) rather than the type of accretor.

6.2.4. Caveats

A few cautionary words are necessary at this point on the cataclysmic variables (CVs), Algol-type binaries, and some LMXBs. For these types of systems, where the $\dot{P}_b$ is detected by looking at the eclipse times in optical data, some selection effects might be present. This means that systems with a $\dot{P}_b$ in line with the theoretical predictions might be more difficult to measure/detect, and therefore the reported values are invariably skewed toward large/anomalous $\dot{P}_b$ values. Something similar also applies to most LMXBs, with the exception of systems where the $\dot{P}_b$ is measured via pulsar timing, in which case the sensitivity of the timing technique potentially allows the detection of values orders of magnitude smaller than those in the CVs and Algol binaries. For the CVs, there is ample literature on the topic, and several different systems with a large $\dot{P}_b$ are reported. In this paper, we include only the T Pyxidis and IM Normae systems, which are the two best-studied cases and have the highest orbital period variation (Patterson et al. 2015, 2016). We also include NN Serpentis (Brinkworth et al. 2006), which is an eclipsing post–common envelope binary where no mass transfer is currently ongoing. We summarize the information on the orbital period evolution of all the binaries discussed in this work in Figure 4. From the figure, it is clear that all sources with short orbital periods that should be losing angular momentum via gravitational-wave emission are evolving on timescales that are at least an order of magnitude shorter than expected. The binaries with wider orbits, where magnetic braking should dominate, also show shorter evolutionary timescales than predicted, although a larger scattering is observed, and some sources are close to the theoretical predictions.

6.3. Models

Since a large number of scenarios are invoked in the literature to explain the orbital evolution of different interacting binaries, it appears legitimate to ask whether it is still possible to find a common (and/or perhaps still unknown) mechanism behind the observed behavior. In the following discussion, we consider all models proposed in the literature and try to apply each of them to the case of SAX J1808.4−3658, with the exception of the third-body model, which has already been excluded (see Section 5.3).

6.3.1. Mass-Loss Model

If the companion star experiences severe mass loss—for example, because of ablation due to the irradiation from a pulsar wind or from the X-rays originating close to the compact object—then the orbital period of the binary changes dramatically (see Section 6.1).

In this case, the orbital period derivative will depend on the amount of mass lost from the companion,

$$\frac{\dot{P}_b}{P_b} = -2\frac{\dot{M}_c}{M_c}, \tag{8}$$

where M_c is the companion mass (see, e.g., Frank et al. 2002; Postnov & Yungelson 2014). Applying this model to SAX J1808.4−3658, it is possible to explain the observed $\dot{P}_b$ if the donor is losing mass at a rate of about $10^{-9}\,M_\odot\,\mathrm{yr}^{-1}$ (di Salvo et al. 2008; but see also Chen 2017).

For the donor to lose a substantial amount of mass, there must be a way to efficiently inject energy into the donor star. Whatever mechanism is chosen, the amount of energy necessary to create such a strong mass loss must be consistent with the total energy budget available to the binary. In SAX J1808.4−3658, it has been proposed that the mass loss is driven by a pulsar wind and high-energy radiation impinging on the donor surface (di Salvo et al. 2008; Burderi et al. 2009). For a circular binary orbit, the total angular momentum is (Frank et al. 2002)

$$J \propto M_{\rm NS} M_c M^{-1/3} P_b^{1/3}, \tag{9}$$

where P_b is the orbital period, $M = M_{\rm NS} + M_c$ is the total binary mass, and $M_c < M_{\rm NS}$. The orbital energy $E_{\rm orb}$ is

$$-E_{\rm orb} \propto J/P_b. \tag{10}$$

From Equation (9), an increase in P_b requires M_c to decrease because, for an isolated system, J and M cannot increase. And, from Equation (10), we see that $-E_{\rm orb}$ must decrease, making the orbit less tightly bound. In other words, an orbital period increase requires energy injection from somewhere. Marsh & Pringle (1990) showed that energy injection by the secondary star is too slow for observed P_b changes, as this is governed by the star's thermal timescale.[13]

The only energy source left is the spin energy of the neutron star. This is

$$E_{\rm spin} \sim k^2\, M_{\rm NS}\, v_K^2 \sim k^2\, GM_{\rm NS}^2/R_{\rm NS}, \tag{11}$$

where k is the radius of gyration, $R_{\rm NS}$ is the physical radius, and $v_K = (GM_{\rm NS}/R_{\rm NS})^{1/2}$ is the breakup spin velocity. This is a huge reservoir, since

$$E_{\rm spin}/(-E) \sim k^2 \frac{M_{\rm NS}}{M_c}\frac{a}{R} \sim 400\text{–}1000 \tag{12}$$

with $k^2 \sim 0.4$. But of course, not all of $E_{\rm spin}$ can be used to drive mass loss from the system and so increase P_b. We can estimate the required minimum efficiency η for spin energy conversion into orbit energy for SAX J1808.4−3658.

The total orbital binding energy of the binary is

$$E_{\rm orb} = -\frac{GM_{\rm NS}M_c}{2a}. \tag{13}$$

If we use the third Kepler law, then we find that the orbital period is very well determined ($P_b = 2.01$ hr, from the X-ray pulse timing). The total mass of the binary is ill constrained, mostly because of the unknown neutron star mass. If we assume a range of total binary mass from 1.4 to 3 $M_\odot$, then the variation in a is of

[13] This is, of course, what happens when a very low-mass star expands on mass transfer ($M_c > M_{\rm NS}$) with $P_b \propto 1/M_c$. The star's thermal energy expands it adiabatically.

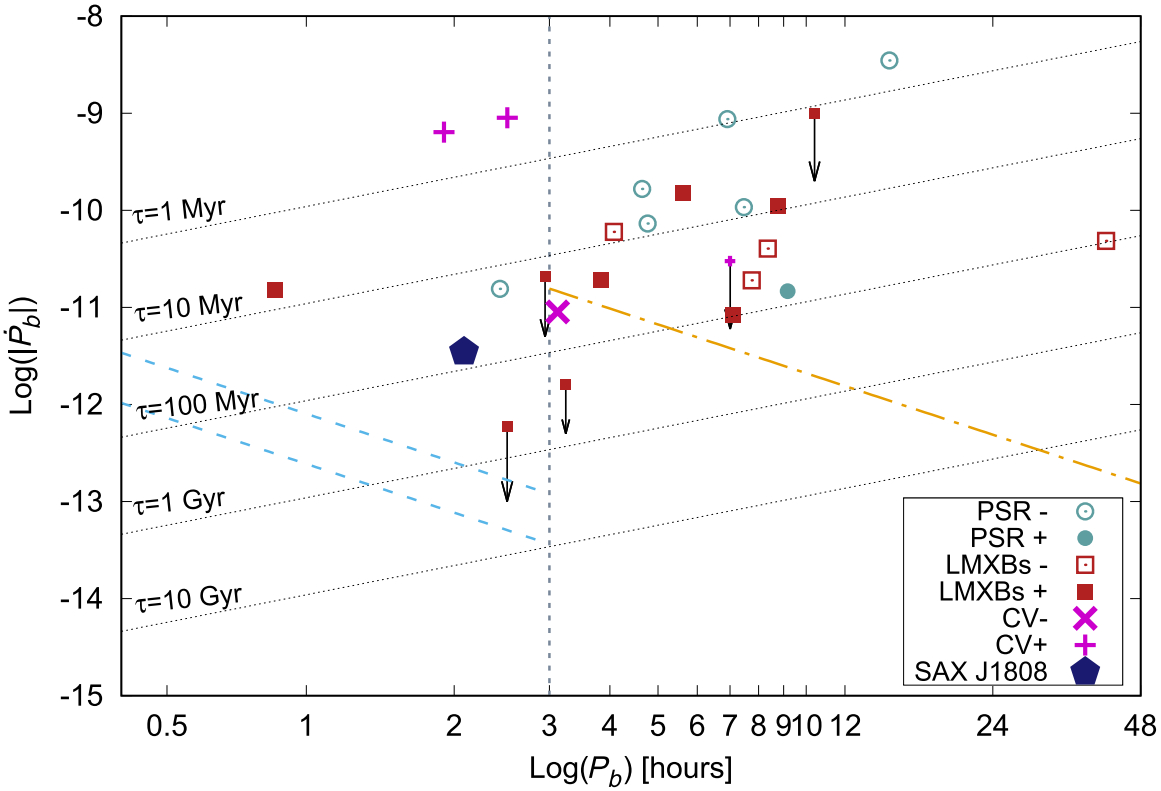

Figure 4. The $|\dot{P}_b|$ vs. P_b diagram for SAX J1808.4−3658 (blue pentagon), LMXBs (red squares), binary pulsars (BWs and redbacks; blue circles), and some CVs (purple crosses). The open symbols identify converging systems (negative $\dot{P}_b$), and filled symbols are diverging ones. Only T Pyx and IM Nor are plotted for CVs (plus NN Ser, which is shown by the same symbol used for CVs). The black dotted lines identify evolutionary timescales $\tau = P_b/|\dot{P}_b|$. The dashed gray line roughly separates the binaries in which the dominant angular momentum loss should be gravitational radiation (left) from those in which magnetic braking is expected to dominate (right), assuming no mass loss or spin–orbit coupling is present in the binary. The cyan dashed lines are the theoretical values of $|\dot{P}_b|$ expected if gravitational-wave emission is the main driver of orbital evolution. From top to bottom, these lines are valid for a donor mass–radius relation $R_c \propto M_c$ and $R_c \propto M_c^{-1/3}$, respectively, assuming adonor mass of 0.08 $M_\odot$ and a neutron star mass of 1.4 $M_\odot$. A value of 0.08 $M_\odot$ has been chosen, as it represents the most likely donor mass in SAX J1808.4−3658. The orange dash-dotted line is the orbital period derivative as a function of orbital period when the maximum possible magnetic-braking effect is considered (see main text for discussion). A mass–radius index $\zeta = 1$ has been assumed for the magnetic-braking case.

the order of 20% (6–8 × 10^{10} cm). Here, we will assume $a = 6.4 \times 10^{10}$ cm ($M_{NS} = 1.4\,M_\odot$, $M_c = 0.08\,M_\odot$). The orbital energy is therefore

$$E_{orb} \sim 3 \times 10^{47}\ \mathrm{erg}. \quad (14)$$

The semimajor axis of the binary changes according to the third Kepler law:

$$\dot{a} = \frac{2a}{3P_b}\dot{P}_b. \quad (15)$$

The value of $\dot{P}_b$ is measured from observations as $\sim 3.5 \times 10^{-12}$. Therefore, $\dot{a} = 2 \times 10^{-5}$ cm s^{-1}. The orbital energy variation is (we assume that $\dot{M}$ terms are negligible)

$$\dot{E}_{orb} = \frac{GM_{NS}M_c\dot{a}}{2\,a^2} \sim 9 \times 10^{31}\ \mathrm{erg\ s^{-1}}. \quad (16)$$

The total spin-down power is

$$\dot{E}_{sd} = I\omega\dot{\omega}, \quad (17)$$

where $\omega = 2\pi\,\nu$, $\dot{\omega} = 2\pi\dot{\nu}$, and ν and $\dot{\nu}$ are the spin frequency (401 Hz) and spin-down (1.65(20) × 10^{-15} Hz s^{-1}) observed in SAX J1808.4−3658 (Patruno et al. 2012). Numerically, $\dot{E}_{sd} \approx 2.6 \times 10^{34}$ erg s^{-1}.

We need an efficiency η of at least the ratio between the two powers:

$$\eta = \frac{\dot{E}_{orb}}{\dot{E}_{sd}} \sim 0.003. \quad (18)$$

For the parameters assumed above, the Roche lobe radius is $R_L = 0.16\,R_\odot$ (see, e.g., Eggleton 1983), and the fraction of intercepted power is $f = (R_L/2a)^2$, which is approximately 0.8%. This value suggests that the donor star must be extremely efficient in converting the incident power into mass loss, since $\epsilon \sim \eta/0.8 \approx 40\%$. Campana et al. (2004) estimated that the irradiating power[14] required to explain the bright optical counterpart of SAX J1808.4−3658 (observed with Very Large Telescope (VLT) data in 2002) amounted to $L_{irr} = 8^{+3}_{-1} \times 10^{33}$ erg s^{-1} (see also Homer et al. 2001 for a similar estimate made with observations taken in 1999). Therefore, the optical data require a conversion of a fraction $\xi = L_{irr}/\dot{E}_{sd} \approx 0.2$–0.6 of incident power into thermal radiation by the donor star (the range provided takes into account the 1σ error bars on the irradiation luminosity and the possibility that the distance is 2.5 kpc rather than 3.5 kpc). Since from the observational constraint we have that $\xi + \epsilon = 0.5$–1.0 and $\xi + \epsilon$ is bound to be equal to 1 by the conservation of energy,

[14] The authors used a distance of 2.5 kpc, whereas we rescale the luminosity for a distance of 3.5 ± 0.1 kpc, as determined by Galloway & Cumming (2006).

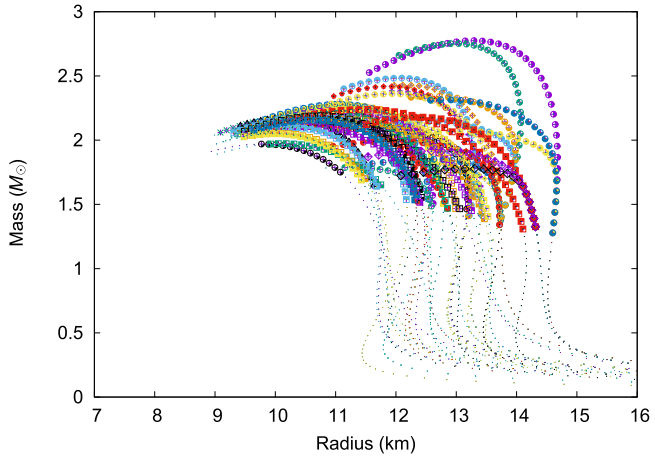

Figure 5. Constraints on the mass–radius relation of the neutron star in SAX J1808.4−3658 under the assumption that the binary is driven by mass loss. The curves correspond to different equations of state of ultra-dense matter and are taken from Fortin et al. (2016). The thick parts of the curves mark the segments for which the moment of inertia of the neutron star is $>1.7 \times 10^{45}$ g cm^2 (see main text for discussion).

this scenario is energetically plausible for a range of parameters compatible with the observations.

If we assume that the mass loss from the donor of SAX J1808.4−3658 is constant, then we still need to explain the $T_{\rm asc}$ of the 2011 outburst. This data point deviated by approximately 7 s from the predicted value that can be obtained in Equation (2) by using a constant $\dot{P}_b = 3.5 \times 10^{-12}$ s s^{-1}. The 7 s deviation can be explained if the mass-loss rate has increased by about ∼70% during the 2008–2011 period, which would require a proportionally larger spin-down power than assumed above. Indeed, the relation between the mass loss and the spin-down power is linear (see, e.g., a discussion in Hartman et al. 2009):

$$\dot{M}_{\rm c} = \dot{E}_{\rm sd}\left(\frac{1}{2a}\right)^2 G\, M_{\rm c}\, R_{\rm c}. \tag{19}$$

Since we have seen that the donor needs to convert the incident spin-down power into mass loss with extraordinary efficiency, close to 40% ($\epsilon \sim 0.4$), the spin-down power is larger than initially estimated, either because of a larger moment of inertia of the neutron star or because the spin-down $\dot{\omega}$ is slightly larger than observed. In the first case, one would need $I \gtrsim 1.7 \times 10^{45}$ g cm^2, and this can be used in principle to constrain the equation of state of ultra-dense matter (under the assumption that mass loss is the main mechanism responsible for the binary evolution). In Figure 5, we plot an illustrative example of the type of constraints that can be obtained when using this method for a selection of equations of state (Fortin et al. 2016).

In conclusion, this mechanism is energetically feasible if

1. SAX J1808.4−3658 has a neutron star with a large moment of inertia and
2. the incident pulsar power can be converted into mass loss with an ≈40% efficiency.

When looking at the whole sample of pulsar binaries, the behavior of other BW pulsars cannot be explained by this model, since at least two of them are shrinking their orbits. Therefore, if the mass-loss model is correct, we need two different mechanisms to explain the population of binary pulsars. Furthermore, in a recent work (Patruno 2016), we studied the orbital evolution of another AMXP, namely, IGR J0029+5934. This system can be considered a "twin" system of SAX J1808.4−3658, since its orbital and physical parameters are extremely similar (see, e.g., Patruno & Watts 2017). However, the orbit of the binary is varying at a very slow pace ($\tau > 0.5$ Gyr), compatible with a conservative scenario in which the binary evolution is driven by gravitational-wave emission. We constrained the efficiency of the pulsar spin-down to mass-loss conversion to be $\lesssim$5%. It is not clear, therefore, why IGR J0029+5934 is unable to convert spin-down power into mass loss, whereas SAX J1808.4−3658 is so efficient. We stress that the observations of both systems suggest a donor irradiated by a pulsar wind/high-energy radiation, and the donor mass is almost identical.

6.3.2. Spin–Orbit Coupling

An exchange of angular momentum between the stellar spin and the orbit can generate variations of the orbital period. These variations of the orbital angular momentum are encoded in the term $\dot{J}_{\rm soc}$ in Equation (6).

The Applegate model was developed by Applegate (1992) and Applegate & Shaham (1994) to explain the orbital variability observed in a sample of eclipsing variables and later applied to the case of the BW pulsar PSR B1957+20 (Applegate & Shaham 1994). The model has been further extended to Roche lobe–filling systems such as cataclysmic variables (Richman et al. 1994). The model can be briefly summarized as follows. If the donor star has internal deformations, then the gravitational potential outside of the active star is (terms higher than quadrupolar are ignored here)

$$\phi(x) = -\frac{GM}{r} - \frac{3}{2} G Q_{ik} \frac{x_i x_k}{r^5}, \tag{20}$$

where x_i and x_k are Cartesian coordinates measured from the center of mass of the star and Q_{ik} is the quadrupole tensor (related to the inertia tensor). For simplicity, one can assume a circular orbit (which is legitimate to do in a binary such as SAX J1808.4−3658), an alignment between the donor spin axis and orbital angular momentum, and that the stellar spin and orbit are synchronized. If the Cartesian system is chosen so that the z-axis is the angular momentum axis and the x-axis points from the center of mass to the companion star, then Q_{ik} reduces to $Q_{xx} = Q$. In a circular orbit, the relative velocity can be written as

$$v^2 = r\frac{d\phi}{dt}. \tag{21}$$

Therefore, from Equation (20), one can see that the relative velocity v is related to the time-varying quadrupole Q. Since v is also related to the orbital period of the binary, it is clear that a time-varying mass quadrupole term induces a variation of the orbital period. Applegate (1992) suggested that the cause of the time-varying quadrupole Q might be related to magnetic cycles of period $P_{\rm mod}$ (in a way analogous to the familiar 11 yr magnetic solar cycles). During these cycles, the magnetic field induces a redistribution of the angular momentum in different layers of the star and allows a transition between different equilibrium configurations. The strength of the surface magnetic field B required to explain a variation ΔP of the

orbital period can be written as

$$B^2 \sim 10\frac{GM^2}{R^4}\left(\frac{A}{R}\right)^2\frac{\Delta P}{P_{\rm mod}}. \quad (22)$$

The transport of angular momentum inside the star of course needs some energy, which Applegate (1992) suggested might come either from the donor internal nuclear burning reservoir or from tidal heating (Applegate & Shaham 1994). This is, in essence, the Applegate model, which has been proposed as a viable way to explain the behavior of many binary systems. It seems therefore natural to extend it to the case of LMXBs. For the case of SAX J1808.4−3658, one needs to assume a value for $P_{\rm mod}$, since the $T_{\rm asc}$ variations observed so far do not show a complete cycle. By assuming $P_{\rm mod} = 50$ yr, $R = 0.1\,R_\odot$, $M = 0.07\,M_\odot$, and $A = 7 \times 10^{10}$ cm, one finds $B \sim 1$ kG.

There are, however, two main problems with the Applegate model applied to SAX J1808.4−3658 and to many other compact binaries considered here. The first is that the required B field is of the order of 1 kG, which is much larger than the typical values thought to be present in fully convective stars. However, some isolated low-mass stars and brown dwarfs have been observed with relatively strong surface B fields (Morin et al. 2010) and, in some cases, with fields larger than 1 kG (Reiners 2012). Furthermore, recent studies have provided observational evidence for the presence of magnetic activity in at least four fully convective stars, suggesting that the dynamo mechanism that produces stellar magnetic fields also operates through convection despite the absence of the tachocline, which is the boundary layer between the radiative and convective envelope where the magnetic fields are generated (Wright & Drake 2016).

The second problem, which seems more difficult to circumvent, was discussed in a critical review by Brinkworth et al. (2006), who found that, for very low-mass stars such as NN Serpentis (which is a nonaccreting, post–common envelope binary with a $0.15\,M_\odot$ companion and an orbital period of 3 hr), the internal energy budget of the donor star might be insufficient to generate the required donor distortion. Even if one invokes the tidal-heating mechanism proposed in Applegate & Shaham (1994), there will still be insufficient energy available to generate the required stellar distortions (see, e.g., Burderi 2015). As was the case for the mass-loss model, the only source of energy left is the spin-down energy of the pulsar. In this case, there needs to be a viable mechanism to transport energy deeper in the donor star that is able to generate a varying-mass quadrupole. As noted by Applegate (1992), if the donor star becomes more oblate, then the mass quadrupole $\Delta Q > 0$ and the orbital period decreases. The opposite happens if $\Delta Q < 0$: the orbital period increases. The observed behavior of most binaries considered in this work might then be explained if, for some reason, some of them (like SAX J1808.4−3658 and other diverging binaries) have $\Delta Q < 0$, whereas all other converging binaries have $\Delta Q > 0$. This idea remains highly speculative, since the problem of what happens in the deep layers of irradiated stars has not been investigated yet.

6.3.3. Enhanced Magnetic Braking

This model could explain the sign and strength of $\dot{P}_b$ in SAX J1808.4−3658 only if the donor magnetic field is sufficiently strong. Indeed, the mass lost by the donor cannot be larger than that estimated in Section 6.3.1, since the energy budget does not allow it. As an example, we follow the recipe provided by Justham et al. (2006), in which the angular momentum lost by the binary via magnetic braking is

$$\dot{J}_{\rm mb} = -\Omega_d\, B_s\, R_c^{13/4}\dot{M}_w^{1/2}(G\,M_c)^{-1/4}, \quad (23)$$

where Ω_d is the angular rotational frequency of the donor star, B_s is its dipolar magnetic field at the surface, and $\dot{M}_w$ is the amount of wind loss. If we assume that SAX J1808.4−3658 is changing orbital parameters mainly because of angular momentum loss, then, by rearranging Equation (5), we obtain

$$\dot{J} = \frac{\dot{a}}{a^{1/2}}M_{\rm NS}M_{\rm c}\left(\frac{G}{M}\right)^{1/2} \approx 2 \times 10^{35}\ {\rm g\ cm^2\ s^{-2}}. \quad (24)$$

Assuming that the donor is tidally locked, Equation (23) gives the strength of the minimum B_s field required, which is of the order of 10^3–10^4 G for a maximum wind-loss rate of $10^{-9}\,M_\odot\,{\rm yr}^{-1}$, even stronger than the value calculated for the Applegate model. This shows that the magnetic-braking model is unlikely to be the correct one. Furthermore, such an explanation cannot work in several other binaries because, at least in some neutron star LMXBs, the sign of the observed orbital period derivative is opposite to that expected when magnetic braking is the main driver of binary evolution.

7. Conclusions

We have studied the AMXP SAX J1808.4−3658 in radio during quiescence in 2014 and in X-rays during its most recent outburst in 2015. We have not detected radio pulsations, and we place strong constraints on the flux density of the putative radio pulsar that, if indeed active, needs to be either among the 10% dimmest pulsars known or fully obscured by radio-absorbing material (which would also be atypical at the relatively high radio-observing frequencies we searched). The study of the orbital evolution of the system has been extended to include the 2015 outburst, and we find two possible interpretations of the data: either the orbit is expanding with stochastic fluctuations around the mean, or the system is shrinking with a change of sign around 2011.

In the first case, the pulsar spin-down power is ablating the companion with an efficiency for the conversion of impinging power to mass loss of the order of 40%.

Alternatively, the Applegate model can explain the behavior of SAX J1808.4−3658 if a strong surface magnetic field of the order of 1 kG is present. The source of energy that powers this field needs to be the spin-down power of the pulsar, but there is no evidence that such large fields exist in the donor star of SAX J1808.4−3658 or that they can be generated by the pulsar wind/high-energy irradiation. This requires further theoretical investigation.

We would like to thank M. Fortin for providing the data for the mass–radius relations of several neutron star models. We would like to thank E. P. J. van den Heuvel for interesting discussions and T. Tauris, J. Verbiest, and Wen-Cong Chen for suggestions. A.P. acknowledges support from an NWO Vidi fellowship. RW was supported by an NWO Top Grant, Module 1. J.W.T.H. is an NWO Vidi Fellow. A.J. and J.W.T.H. acknowledge funding from the European Research Council under the European Union's Seventh Framework Programme (FP7/2007-2013)/ERC grant agreement number 337062 (DRAGNET). Some of the results

presented in this paper were based on observations obtained with the GBT+GUPPI. We would therefore like to express our gratitude toward the National Radio Astronomy Observatory (NRAO)—a facility of the United States National Science Foundation (NSF)—responsible for operating the GBT. Computational support for radio data analysis was provided by supercomputer Cartesius, a service offered by the Dutch SURFsara. Some of the scientific results reported in this article are based on observations made with the *Chandra X-ray Observatory*. This research has made use of software provided by the *Chandra* X-ray Center (CXC) in the application package CIAO.

References

Altamirano, D., Casella, P., Patruno, A., Wijnands, R., & van der Klis, M. 2008, ApJL, 674, L45
Applegate, J. H. 1992, ApJ, 385, 621
Applegate, J. H., & Shaham, J. 1994, ApJ, 436, 312
Archibald, A. M., Bogdanov, S., Patruno, A., et al. 2015, ApJ, 807, 62
Archibald, A. M., Kaspi, V. M., Hessels, J. W. T., et al. 2013, arXiv:1311.5161
Archibald, A. M., Stairs, I. H., Ransom, S. M., et al. 2009, Sci, 324, 1411
Bailes, M., Bates, S. D., Bhalerao, V., et al. 2011, Sci, 333, 1717
Bassa, C. G., Patruno, A., Hessels, J. W. T., et al. 2014, MNRAS, 441, 1825
Bates, S. D., Lorimer, D. R., & Verbiest, J. P. W. 2013, MNRAS, 431, 1352
Bhattacharya, D. 1998, in NATO Advanced Science Institutes (ASI) Series C, Vol. 515, ed. R. Buccheri, J. van Paradijs, & A. Alpar (Dordrecht: Kluwer), 103
Bildsten, L., & Chakrabarty, D. 2001, ApJ, 557, 292
Breton, R. P., van Kerkwijk, M. H., Roberts, M. S. E., et al. 2013, ApJ, 769, 108
Brinkworth, C. S., Marsh, T. R., Dhillon, V. S., & Knigge, C. 2006, MNRAS, 365, 287
Bult, P., & van der Klis, M. 2015, ApJ, 806, 90
Burderi, L. 2015, EWASS Symposium 11, Is Radio-Ejection ubiquitous among Accreting Millisecond Pulsar (Tenerife: EWASS), 1247
Burderi, L., Di Salvo, T., D'Antona, F., Robba, N. R., & Testa, V. 2003, A&A, 404, L43
Burderi, L., Di Salvo, T., Riggio, A., et al. 2010, A&A, 515, A44
Burderi, L., Possenti, A., D'Antona, F., et al. 2001, ApJL, 560, L71
Burderi, L., Riggio, A., di Salvo, T., et al. 2009, A&A, 496, L17
Cackett, E. M., Altamirano, D., Patruno, A., et al. 2009, ApJL, 694, L21
Campana, S., D'Avanzo, P., Baglio, C., Zelati, F. C., & Kennea, J. 2015, ATel, 7379, 1
Campana, S., D'Avanzo, P., Casares, J., et al. 2004, ApJL, 614, L49
Campana, S., Stella, L., & Kennea, J. A. 2008, ApJL, 684, L99
Cantrell, A. G., Bailyn, C. D., Orosz, J. A., et al. 2010, ApJ, 710, 1127
Chakrabarty, D., & Morgan, E. H. 1998, Natur, 394, 346
Chen, W.-C. 2017, MNRAS, 464, 4673
Chou, Y., Hsieh, H.-E., Hu, C.-P., Yang, T.-C., & Su, Y.-H. 2016, arXiv:1608.04190
Cordes, J. M., & Lazio, T. J. W. 2002, arXiv:astro-ph/0207156
Cordes, J. M., & Lazio, T. J. W. 2003, arXiv:astro-ph/0301598
Courvoisier, T. J.-L., Walter, R., Beckmann, V., et al. 2003, A&A, 411, L53
Deloye, C. J., Heinke, C. O., Taam, R. E., & Jonker, P. G. 2008, MNRAS, 391, 1619
de Oña Wilhelmi, E., Papitto, A., Li, J., et al. 2016, MNRAS, 456, 2647
Dewey, R. J., Taylor, J. H., Weisberg, J. M., & Stokes, G. H. 1985, ApJL, 294, L25
di Salvo, T., Burderi, L., Riggio, A., Papitto, A., & Menna, M. T. 2008, MNRAS, 389, 1851
Doroshenko, O., Löhmer, O., Kramer, M., et al. 2001, A&A, 379, 579
DuPlain, R., Ransom, S., Demorest, P., et al. 2008, Proc. SPIE, 7019, 70191D
Eggleton, P. P. 1983, ApJ, 268, 368
Erdem, A., & Öztürk, O. 2014, MNRAS, 441, 1166
Evans, P. A., Beardmore, A. P., Page, K. L., et al. 2007, A&A, 469, 379
Evans, P. A., Beardmore, A. P., Page, K. L., et al. 2009, MNRAS, 397, 1177
Fortin, M., Providência, C., Raduta, A. R., et al. 2016, PhRvC, 94, 035804
Frank, J., King, A., & Raine, D. J. 2002, in Accretion Power in Astrophysics, ed. J. Frank, A. King, & D. Raine (3rd.; Cambridge, UK: Cambridge Univ. Press), 398
Galloway, D. K., & Cumming, A. 2006, ApJ, 652, 559
Gambino, A. F., Iaria, R., Di Salvo, T., et al. 2016, A&A, 589, A34
Gavriil, F. P., Strohmayer, T. E., Swank, J. H., & Markwardt, C. B. 2007, ApJL, 669, L29
Gierliński, M., Done, C., & Barret, D. 2002, MNRAS, 331, 141
Goldwurm, A., David, P., Foschini, L., et al. 2003, A&A, 411, L223
González Hernández, J. I., Rebolo, R., & Casares, J. 2012, ApJL, 744, L25
González Hernández, J. I., Rebolo, R., & Casares, J. 2014, MNRAS, 438, L21
González Hernández, J. I., Suárez-Andrés, L., Rebolo, R., & Casares, J. 2017, MNRAS, 465, L15
Hartman, J. M., Patruno, A., Chakrabarty, D., et al. 2008, ApJ, 675, 1468
Hartman, J. M., Patruno, A., Chakrabarty, D., et al. 2009, ApJ, 702, 1673
Heinke, C. O., Grindlay, J. E., Edmonds, P. D., et al. 2005, ApJ, 625, 796
Heinke, C. O., Jonker, P. G., Wijnands, R., Deloye, C. J., & Taam, R. E. 2009, ApJ, 691, 1035
Hobbs, G. B., Edwards, R. T., & Manchester, R. N. 2006, MNRAS, 369, 655
Homer, L., Charles, P. A., Chakrabarty, D., & van Zyl, L. 2001, MNRAS, 325, 1471
Hu, C.-P., Chou, Y., & Chung, Y.-Y. 2008, ApJ, 680, 1405
Iacolina, M. N., Burgay, M., Burderi, L., Possenti, A., & di Salvo, T. 2010, A&A, 519, A13
Iaria, R., di Salvo, T., Burderi, L., et al. 2011, A&A, 534, A85
Iaria, R., Di Salvo, T., Gambino, A. F., et al. 2015, A&A, 582, A32
in't Zand, J. J. M., Heise, J., Muller, J. M., et al. 1998, A&A, 331, L25
Jain, C., & Paul, B. 2011, MNRAS, 413, 2
Jain, C., Paul, B., & Dutta, A. 2010, MNRAS, 409, 755
Jaodand, A., Archibald, A. M., Hessels, J. W. T., et al. 2016, ApJ, 830, 122
Joshi, K. J., & Rasio, F. A. 1997, ApJ, 479, 948
Justham, S., Rappaport, S., & Podsiadlowski, P. 2006, MNRAS, 366, 1415
Knigge, C., Baraffe, I., & Patterson, J. 2011, ApJS, 194, 28
Knigge, C., King, A. R., & Patterson, J. 2000, A&A, 364, L75
Lazaridis, K., Verbiest, J. P. W., Tauris, T. M., et al. 2011, MNRAS, 414, 3134
Lazarus, P., Brazier, A., Hessels, J. W. T., et al. 2015, ApJ, 812, 81
Lebrun, F., Leray, J. P., Lavocat, P., et al. 2003, A&A, 411, L141
Lorimer, D. R. 2008, LRR, 11, 8
Lorimer, D. R., & Kramer, M. 2012, Handbook of Pulsar Astronomy (Cambridge: Cambridge Univ. Press)
Manchester, R. N., Hobbs, G. B., Teoh, A., & Hobbs, M. 2005, AJ, 129, 1993
Marsh, T. R., & Pringle, J. E. 1990, ApJ, 365, 677
Morin, J., Donati, J.-F., Petit, P., et al. 2010, MNRAS, 407, 2269
Nice, D. J., Arzoumanian, Z., & Thorsett, S. E. 2000, in ASP Conf. Ser. 202, IAU Coll. 177: Pulsar Astronomy—2000 and Beyond, ed. M. Kramer, N. Wex, & R. Wielebinski (San Francisco, CA: ASP), 67
Papitto, A., di Salvo, T., D'Aı, A., et al. 2009, A&A, 493, L39
Papitto, A., Ferrigno, C., Bozzo, E., et al. 2013, Natur, 501, 517
Patruno, A. 2016, arXiv:1611.06055
Patruno, A., Altamirano, D., Hessels, J. W. T., et al. 2009a, ApJ, 690, 1856
Patruno, A., Bult, P., Gopakumar, A., et al. 2012, ApJL, 746, L27
Patruno, A., Hartman, J. M., Wijnands, R., Chakrabarty, D., & van der Klis, M. 2010, ApJ, 717, 1253
Patruno, A., Maitra, D., Curran, P. A., et al. 2016, ApJ, 817, 100
Patruno, A., Rea, N., Altamirano, D., et al. 2009b, MNRAS, 396, L51
Patruno, A., Watts, A., Klein Wolt, M., Wijnands, R., & van der Klis, M. 2009c, ApJ, 707, 1296
Patruno, A., & Watts, A. L. 2017, ApJ, 839, 51
Patterson, J., Monard, B., Warhurst, P., & Myers, G. 2015, JAVSO, 43, 259
Patterson, J., Oksanen, A., Kemp, J., et al. 2016, MNRAS, 466, 581
Paul, B., & Jain, C. 2010, in The First Year of MAXI: Monitoring Variable X-ray Sources, 26, http://maxi.riken.jp/FirstYear
Perera, B. B. P., Stappers, B. W., Lyne, A. G., et al. 2017, MNRAS, 468, 2114
Pletsch, H. J., & Clark, C. J. 2015, ApJ, 807, 18
Ponti, G., De, K., Munoz-Darias, T., Stella, L., & Nandra, K. 2017, MNRAS, 464, 840
Postnov, K. A., & Yungelson, L. R. 2014, LRR, 17, 3
Poutanen, J., & Gierliński, M. 2003, MNRAS, 343, 1301
Ransom, S. M. 2001, PhD thesis, Harvard Univ.
Ransom, S. M., Cordes, J. M., & Eikenberry, S. S. 2003, ApJ, 589, 911
Ransom, S. M., Eikenberry, S. S., & Middleditch, J. 2002, AJ, 124, 1788
Ransom, S. M., Greenhill, L. J., Herrnstein, J. R., et al. 2001, ApJL, 546, L25
Rappaport, S., Joss, P. C., & Webbink, R. F. 1982, ApJ, 254, 616
Rappaport, S., Ma, C. P., Joss, P. C., & Nelson, L. A. 1987, ApJ, 322, 842
Rappaport, S., Verbunt, F., & Joss, P. C. 1983, ApJ, 275, 713
Reiners, A. 2012, LRSP, 9, 1
Richman, H. R., Applegate, J. H., & Patterson, J. 1994, PASP, 106, 1075
Roberts, M. S. E. 2013, in IAU Symp. 291, ed. J. van Leeuwen (Cambridge: Cambridge Univ. Press), 127
Roy, J., Ray, P. S., Bhattacharyya, B., et al. 2015, ApJL, 800, L12
Rutledge, R. E., Fox, D. W., Kulkarni, S. R., et al. 2004, ApJ, 613, 522

Sanna, A., Burderi, L., Riggio, A., et al. 2016, MNRAS, 459, 1340
Sanna, A., Riggio, A., Pintore, F., et al. 2015, ATel, 7364, 1
Scholz, P., Kaspi, V. M., Lyne, A. G., et al. 2015, ApJ, 800, 123
Shaifullah, G., Verbiest, J. P. W., Freire, P. C. C., et al. 2016, MNRAS, 462, 1029
Skumanich, A. 1972, ApJ, 171, 565
Spruit, H. C., & Ritter, H. 1983, A&A, 124, 267
Stappers, B. W., Bailes, M., Lyne, A. G., et al. 2001, MNRAS, 321, 576
Staubert, R., Klochkov, D., & Wilms, J. 2009, A&A, 500, 883
Stepien, K. 1995, MNRAS, 274, 1019
Tauris, T. M. 2011, in ASP Conf. Ser. 447, Evolution of Compact Binaries, ed. L. Schmidtobreick, M. R. Schreiber, & C. Tappert (San Francisco, CA: ASP), 285
Tauris, T. M., & van den Heuvel, E. P. J. 2006, in Compact Stellar X-ray Sources, ed. W. H. G. Lewin & M. van der Klis (Cambridge: Cambridge Univ. Press), 623
Taylor, J. H., & Weisberg, J. M. 1989, ApJ, 345, 434
Thorsett, S. E., Arzoumanian, Z., Camilo, F., & Lyne, A. G. 1999, ApJ, 523, 763
Ubertini, P., Lebrun, F., Di Cocco, G., et al. 2003, A&A, 411, L131
van der Klis, M. 1995, in The Lives of the Neutron Stars, ed. M. A. Alpar, U. Kiziloglu, & J. van Paradijs (Dordrecht: Kluwer), 301
van der Klis, M. 2000, ARA&A, 38, 717
van der Sluys, M. 2011, in ASP Conf. Ser. 447, Evolution of Compact Binaries, ed. L. Schmidtobreick, M. R. Schreiber, & C. Tappert (San Francisco, CA: ASP), 317
van Teeseling, A., & King, A. R. 1998, A&A, 338, 957
Verbunt, F. 1993, ARA&A, 31, 93
Wang, Z., Breton, R. P., Heinke, C. O., Deloye, C. J., & Zhong, J. 2013, ApJ, 765, 151
Weisberg, J. M., & Taylor, J. H. 2002, ApJ, 576, 942
Wijnands, R., Méndez, M., Markwardt, C., et al. 2001, ApJ, 560, 892
Wijnands, R., & van der Klis, M. 1998, Natur, 394, 344
Wijnands, R., van der Klis, M., Homan, J., et al. 2003, Natur, 424, 44
Winkler, C., Courvoisier, T. J.-L., Di Cocco, G., et al. 2003, A&A, 411, L1
Wolff, M. T., Hertz, P., Wood, K. S., Ray, P. S., & Bandyopadhyay, R. M. 2002, ApJ, 575, 384
Wolff, M. T., Ray, P. S., Wood, K. S., & Hertz, P. L. 2009, ApJS, 183 156
Wolszczan, A. 1994, Sci, 264, 538
Wolszczan, A., & Frail, D. A. 1992, Natur, 355, 145
Wright, N. J., & Drake, J. J. 2016, Natur, 535, 526
Xing, Y., Wang, Z., & Jithesh, V. 2015, arXiv:1502.00733
Yagi, K. 2012, PhRvD, 86, 081504